ASTROBIOLOGY
Volume 8, Number 1, 2008

DOI: 10.1089/ast.2006.0037

Research Paper

Identification of Morphological Biosignatures in Martian Analogue Field Specimens Using *In Situ* Planetary Instrumentation

DEREK PULLAN,[1] FRANCES WESTALL,[2] BEDA A. HOFMANN,[3] JOHN PARNELL,[4] CHARLES S. COCKELL,[5] HOWELL G.M. EDWARDS,[6] SUSANA E. JORGE VILLAR,[7] CHRISTIAN SCHRÖDER,[8] GORDON CRESSEY,[9] LUCIA MARINANGELI,[10] LUTZ RICHTER,[11] and GÖSTAR KLINGELHÖFER[8]

ABSTRACT

We have investigated how morphological biosignatures (*i.e.*, features related to life) might be identified with an array of viable instruments within the framework of robotic planetary surface operations at Mars. This is the first time such an integrated lab-based study has been conducted that incorporates space-qualified instrumentation designed for combined *in situ* imaging, analysis, and geotechnics (sampling).

Specimens were selected on the basis of feature morphology, scale, and analogy to Mars rocks. Two types of morphological criteria were considered: potential signatures of extinct life (fossilized microbial filaments) and of extant life (crypto-chasmoendolithic microorganisms). The materials originated from a variety of topical martian analogue localities on Earth, including impact craters, high-latitude deserts, and hydrothermal deposits.

Our *in situ* payload included a stereo camera, microscope, Mössbauer spectrometer, and sampling device (all space-qualified units from Beagle 2), and an array of commercial instruments, including a multi-spectral imager, an X-ray spectrometer (calibrated to the Beagle 2 instrument), a micro-Raman spectrometer, and a bespoke (custom-designed) X-ray diffractometer. All experiments were conducted within the engineering constraints of *in situ* operations to generate realistic data and address the practical challenges of measurement.

[1]Space Research Centre, Department of Physics and Astronomy, University of Leicester, Leicester, UK.
[2]Centre de Biophysique Moléculaire, CNRS, Orléans, France.
[3]Natural History Museum, Bern, Switzerland.
[4]Department of Geology, University of Aberdeen, Aberdeen, UK.
[5]Planetary and Space Sciences Research Institute, The Open University, Milton Keynes, UK.
[6]Department of Chemical and Forensic Sciences, School of Life Sciences, University of Bradford, Bradford, UK.
[7]Area de Geodinamica Interna, Facultad de Humanidades y Educacion, Universidad de Burgos, Burgos, Spain.
[8]Institut für Anorganische und Analytische Chemie, Johannes Gutenberg-Universität, Mainz, Germany.
[9]Department of Mineralogy, Natural History Museum, London, UK.
[10]International Research School of Planetary Sciences, Dipartimento di Scienze, Università d'Annunzio, Pescara, Italy.
[11]Deutsches Zentrum für Luft- und Raumfahrt (DLR), Institute of Space Simulation, Cologne, Germany.

Our results demonstrate the importance of an integrated approach for this type of work. Each technique made a proportionate contribution to the overall effectiveness of our "pseudo-payload" for biogenic assessment of samples yet highlighted a number of limitations of current space instrument technology for *in situ* astrobiology. Key Words: Analogue—*In situ* measurement—Biosignatures—Planetary instrumentation—Mars. Astrobiology 8, 119–156.

INTRODUCTION

ROBOTIC SPACECRAFT deployed at a planet's surface and equipped with imaging, analytical, and geotechnical (*i.e.*, sampling) capabilities have demonstrated the effectiveness of remote *in situ* geological site investigation (Squyres and Knoll, 2005, and references therein). With increasing demand for extra mobility and autonomy (Gilmore *et al.*, 2000; Schenker *et al.*, 2003), a wide variety of spatial and spectral capabilities of imaging instruments will likely be required to span the entire scale range for future missions. In addition, fundamental analytical measurements remain crucial for establishing reliable ground truth and essential geological context (Clark *et al.*, 2005). Similarly, versatile and effective sample preparation and acquisition methods are potential determinants of success, especially for missions with life-detection or sample-return objectives, or both (Richter *et al.*, 2002; Gorevan *et al.*, 2003a). Suitably equipped payloads could, therefore, play an important role in the access to, and identification of, direct or indirect visual indicators of life, if such features exist at the planetary surface or in the subsurface.

Our work forms part of a wider program of integrated and multidisciplinary studies that address the practicalities of *in situ* measurements at planetary surfaces (PAFSnet*). In this paper, we focus on morphological biosignatures (bona fide microfossils and extant endolithic microorganisms) and assess the ability of current space instrument technology to identify such features within the framework of future robotic planetary surface operations.

For the purposes of this study, a modest number of geological specimens from our archive of planetary analogues were selected on the basis of analogy, scale, and morphological feature type (Table 1). Instrumentation and techniques available to us included flight spare assets from the Beagle 2 Mars lander (Pullan *et al.*, 2003), including a single camera from the Stereo Camera System, microscope, Mössbauer spectrometer, X-ray spectrometer (XRS), and a soil-sampling device (*aka* PLUTO). In addition, selected commercial equipment served as emulators of potential future instruments currently being developed for space, including a multi-spectral imager (CR-i Nuance system), a micro-Raman spectrometer (Bruker NIR non-confocal and Renishaw VNIR/VIS Raman microscopes), and an *in situ* X-ray diffractometer (Natural History Museum, London). Other techniques recently introduced to our repertoire will be incorporated in follow-up studies, including post-sampling immunoassay for biomarker detection (Sims *et al.*, 2005).

Mobility, vision, dexterity, and the ability to perform analytical tasks are as much prerequisites for planetary robots as they are for terrestrial scientists working in the field. Unfortunately, all space-borne payloads are constrained by engineering and mission resources, so selection of appropriate instrumentation to maximize scientific return will always be balanced between the primary objective and spacecraft limitations. We conduct all our experiments mindful of these constraints.

Within our program of studies (including this one), we do not seek to confine ourselves to a particular payload configuration or mission or indeed make specific instrument recommendations for future missions. Our aim is to adopt an unbiased, unified approach to *in situ* exploration through practical experimentation by way of a broad range of techniques in order to establish a knowledge base that will be beneficial to the community well in advance of operations at the planetary surface.

Scientific perspective

If life once existed on Mars or, indeed, if it still exists there, to what form it evolved and whether evidence (visual or otherwise) is preserved in the

*The Planetary Analogue Field Studies Network (PAFSnet) is a multidisciplinary group of scientists and engineers with a common interest in planetary exploration and thematic studies incorporating terrestrial analogues in the laboratory and in the field (see www.pafsnet.org).

TABLE 1. STUDY SAMPLE CHARACTERISTICS AND ANALOGOUS ASSOCIATIONS

Sample	*Characteristics**
Limestone 1,a,c,d,g,j	Freshwater crater lake deposit; combination of open fabric and sintered surfaces; high microscopic relief on the former; dolomitic matrix and veneers; calcified *Cladophorites* filaments, hollow tubular morphology; aligned, clustered; individual tubes mm to cm long and ~100 μm outer diameter. Masses extend to cm; family ID 140.
Opaline sinter 2,a,c,f,j	Hot spring precipitate (siliceous sinter), microbial mat replacement product; silicified filament-filled voids; high microscopic relief; individual filaments typically ~15 μm wide and <500 μm long; family ID 169.
Chalcedony 3,a,c,i	Hydrothermal vein; Fe-encrusted filaments in late stage chalcedony; moderate microscopic relief; encrusted filaments ~200 μm wide and extend to cm; family ID 45.
Goethite 4,a,c,h,i	Heavy metal precipitate; Fe-encrusted filaments, generally aligned, locally chaotic; "wood-like" appearance, open fabric; high microscopic relief; individual filaments typically 100 μm wide and mm to cm long; family ID 179.
Orthoquartzite 5,b,c,e,j	Exfoliated sandstone; case-hardened discolored exterior; cryptoendoliths (lichens and microalgae), vertical zonation to few cm; Fe mobilization; low microscopic relief; family ID 114.
Marble 5,b,c,e,j	Crystalline rock; low microscopic relief; weathered surface slightly oxidized; chasmoliths (cyanobacteria) on fresh and internal weathered surfaces exhibit biofluorescence; colonies extend to cm and consist of a patchwork of "globules" typically 50–100 μm diameter; family ID 194.
Selenite 6,b,c,d,j	Post-impact remobilized sulfate; large cleavage folia; low surface relief but "high" microscopic relief due to transparency; interlaminar chasmoliths (*Nostoc* and *Gloeocapsa*); clusters typically few mm across and often chained together into larger communities; family ID 44.

Source locality

1. Hainsfarth, Ries Crater, Germany
2. Hillside Springs, Yellowstone Park, Wyoming, USA
3. Cady Mountains, Mojave Desert, California, USA
4. Cerro de Pasco, Peru
5. McMurdo Dry Valleys, Victoria Land, Antarctica
6. Haughton Crater, Devon Island, Canada

Category codes

a. Microbial filamentous morphology
b. Recent or modern (currently active) extreme biohabitat
c. Macroscopic/microscopic morphological biosignatures
d. Impact crater site
e. Cold-dry valley environment
f. Hot spring environment
g. Aqueous environment
h. Oxidation zone of hydrothermal ore deposit
i. Formed at depth (meters) below solid surface
j. Formed on or just below solid surface (includes endoliths)

*Family ID (see text).

rock record remains unknown. What we might plausibly find in terms of morphological evidence can, at least initially, be guided by analogy to terrestrial systems (Friedmann *et al*., 1988; Hofmann and Farmer, 2000; Cockell and Lee, 2002; Bishop *et al*., 2004; Westall, 2005a) and what has been observed so far on Mars (or has not been observed, as the case may be) (Squyres and Knoll, 2005; Knoll *et al*., 2005; Des Marais *et al*., 2005).

The lithologies observed at Meridiani Planum exhibit cross-bedding and a sub-aqueous history (Squyres and Knoll, 2005) but are thought to offer little preservation potential for organics (Sumner, 2004). More suitable targets for *in situ* astrobiological investigations of organic biosignatures may be clay-rich deposits, cherts, and carbonates. Phyllosilicates have recently been detected in several regions of Mars (Poulet *et al*., 2005), and

silica-rich deposits have been inferred from THEMIS data in Eos Chasma (Hamilton, 2006) and recently observed by Spirit in Gusev Crater. Although carbonates have yet to be identified on Mars, they still warrant analogous study in advance of potential discovery.

Morphology alone does not always allow for the determination of biogenic origin (Cady *et al*., 2003; Ruiz *et al*., 2002; Westall, 2005b). Stromatolites, for example, are generally considered to be microbially mediated sedimentary structures (Walter, 1978; Krumbein, 1983), but in the ancient rock record, the biogenic origin of some stromatolite-like structures is questioned (*e.g*., Lowe, 1980; Walter *et al*., 1980; Hofmann *et al*., 1999; Awramik and Grey, 2005) or disputed (Lowe, 1994; Grotzinger and Rothman, 1996; Grotzinger and Knoll, 1999). Nevertheless, such features would still require *in situ* analysis to confirm their biogenicity (followed by further analysis on Earth in the case of a sample-return mission). Conversely, the absence of organics in samples that express morphological features does not necessarily prohibit the identification of a biosignature if reasonable supporting evidence is available. For example, mineral-encrusted cyanobacterial filaments from Yellowstone hot springs demonstrate morphological characteristics that are clearly biogenic, yet the organic matter has been completely oxidized (Cady and Farmer, 1996).

Clearly, evidence needs to be accumulated using different methods in order to corroborate the involvement of biota in any potential candidate feature observed via imaging techniques (Boston *et al*., 2001; Westall, 2005b). Multi-scale/multispectral imaging forms the basis for initial reconnaissance of candidate targets. In the case of hidden signatures (*i.e*., signatures existing within the fabric of rocks), indirect evidence may be all that is at hand. Expending precious mission resources to split a rock open will be a challenging decision and may be based on subtle textural or spectral anomalies of external weathered surfaces, or both. Analytical instruments play a crucial role by measuring specific characteristics of the material under scrutiny. Such measurements establish context, minimize ambiguity, and provide direction for adopting best sampling strategies.

Instrumentation perspective

With reducing scale, natural materials such as rocks and soils often become more complex in both physical relief and composition. Heterogeneity and homogeneity can change significantly with varying fields of view (FOV). It follows, therefore, that "seamless" imaging (spatial and spectral) is important since target selection becomes more crucial, especially if the morphological biosignatures in question are small, subtle, isolated, or even hidden. To compound the problem, we have to consider the constraints placed upon us by robotic engineering in terms of positional accuracy, accessibility, and dexterity at ever finer scales.

It is unlikely that deployable imaging instruments would be able to scrutinize material at the nanometric scale without sophisticated infrastructure. At such scales, targeting becomes more reliant on positioning and sampling accuracy. Nanometric measurements are more achievable within the sample processing chain of an onboard laboratory, but this, of course, would be after commitment to sampling.

From a purely instrumentation perspective (*i.e*., independent of the planetary analogue theme), target feature parameters such as geometry, scale, organic content, color and spectral contrast, and host parameters such as chemistry, mineralogy, texture, fabric, weathered state, and physical properties define a generic set of variables for *in situ* characterization. The full capability of any instrument or tool needs to be evaluated against these variables independently and in concert with other elements of a payload suite.

MATERIALS AND METHODS

The specimens selected for this study exhibit morphological features related to or mediated by biology. All were obtained from planetary (martian) analogue field sites on Earth, including modern high-latitude extreme environments and Tertiary (~10–39 Ma) crater lake/hydrothermal deposits. Samples broadly fall into 2 morphological categories: fossilized microbial filaments and endolithic microbial communities (Table 1). Physical specimens are referenced by their simplified database identifier <familyID><formatID><itemID> (see www.pafsnet.org for details).

Observable features range in size between submillimeter and a few centimeters. The preservation states on different surfaces of each specimen range from pristine (fresh) to degraded (weath-

ered). Such a collection of specimens presents an interesting array of different, yet relevant, challenges for the *in situ* instrumentation and methods used in the study. Moreover, these examples provide an opportunity to evaluate scientific strategies for justifying targets for subsequent sampling.

Microbial filaments

Specimens that contain fossilized microbial filaments exhibit microscopic morphology (isolated individuals) or macroscopic morphology (communities/assemblages), or both. To provide chemo-mineralogical variation, 3 modes of preservation are included: calcification (freshwater limestone), silicification (opaline sinter and chalcedony), and heavy metal precipitation (goethite). The samples represent 3 different environmental settings: an impact crater lake, a surface hot spring, and subsurface hydrothermal deposits.

Freshwater limestone, Hainsfarth, Ries Crater, Germany (140)

The Ries and Steinheim craters of the Jurassic Alb plateau in Southern Germany represent well-studied examples of terrestrial impact structures (Pohl *et al*., 1977; Pache *et al*., 2001). Near-shore crater lake carbonates are well exposed at Büschelberg near Hainsfarth (48°57.15′N, 10°38.1′E), 2.5 km east of Öttingen, and have been extensively studied (Arp, 1995). The carbonate sequence is thick (>8 m) and consists of extensive bioherms of *Cladophorites* (green algae) with minor stromatolites and carbonate sands composed of gastropods and ostracods. The carbonates lie directly on basal suevite.

The specimens represent a combination of well-preserved (fresh) and weathered calcified remnants of *Cladophorites* cemented in a dolomite matrix (Fig. 1a). The tubular morphology is due to the precipitation of a carbonate crust around the original *Cladophorites* threads, which were subsequently completely oxidized, thus leaving a void (compare Cady and Farmer, 1996) (Figs. 9 and 11). This, together with sinter-like crusts on associated algal constructions within the bioherm, suggests that temporal vadose conditions prevailed where evaporation may have led to impregnation of carbonate into the biofilms (Arp, 2005, personal communication). Subsequent phreatic conditions during the Upper Miocene dolomitized these carbonates, and most surfaces are veneered with dolomite cement. Although the visible calcified tubes no longer contain carbonaceous remains, their morphological characteristics (resulting from mineralization over a *Cladophorites* substrate) classify them as biosignatures.

Opaline Sinter, Yellowstone Park, Wyoming, USA (169)

Yellowstone Park is well known for geysers, fumaroles, hot springs, and associated thermophilic life (Cady and Farmer, 1996; Fouke *et al*., 2000; Rothschild and Mancinelli, 2001; Lowe and Braunstein, 2003; Walker *et al*., 2005). Hillside Springs (44°28.30′N, 110°51.8′W) is located 3.5 km northwest of Old Faithful geyser in the Upper Geyser Basin area. Unusually, the springs discharge from a steep mountain slope approximately 20 m above the valley floor (hence the name Hillside). Discharge temperatures of 82–85°C were recorded by one of us (Hofmann) in September 1996. Fluids are rich in silica and carbonate, which precipitate out to form siliceous and carbonate-rich deposits. Minor constituents also include montmorillonite-group clay minerals (nontronite) and hollandite (Ba-rich Mn-hydroxide). Inevitably, microbial communities living at the surface/fluid interface can become preserved as relict micro-fabric within the rock.

The study specimens were collected by a research team led by Jack Farmer (NASA Ames Research Center) in 1995. They are representative of a hot spring precipitate that is comprised almost entirely of silica and has replaced a microbial mat. The specimens have a macroscopically distinct layered fabric that consists of alternating flat parallel layers and layers with a vertical texture (Fig. 1b). Pore space is very high with voids (up to 10 mm) that are occupied by fibrous structures (Fig. 13) similar in microfabric to *Phormidium*, a sheathed cyanobacterium that usually forms flat, slimy mats of tangled filaments at temperatures between 35 and 59°C at some distance from the spring source (Cady and Farmer, 1996). The observed "threads" (Fig. 13d) are not thought to be the individual filaments themselves (which are usually <5 μm across) but are considered to be representative of a larger preserved biofabric that consists of bundles of filaments. Nevertheless, the overall morphology can be considered as a preserved biosignature.

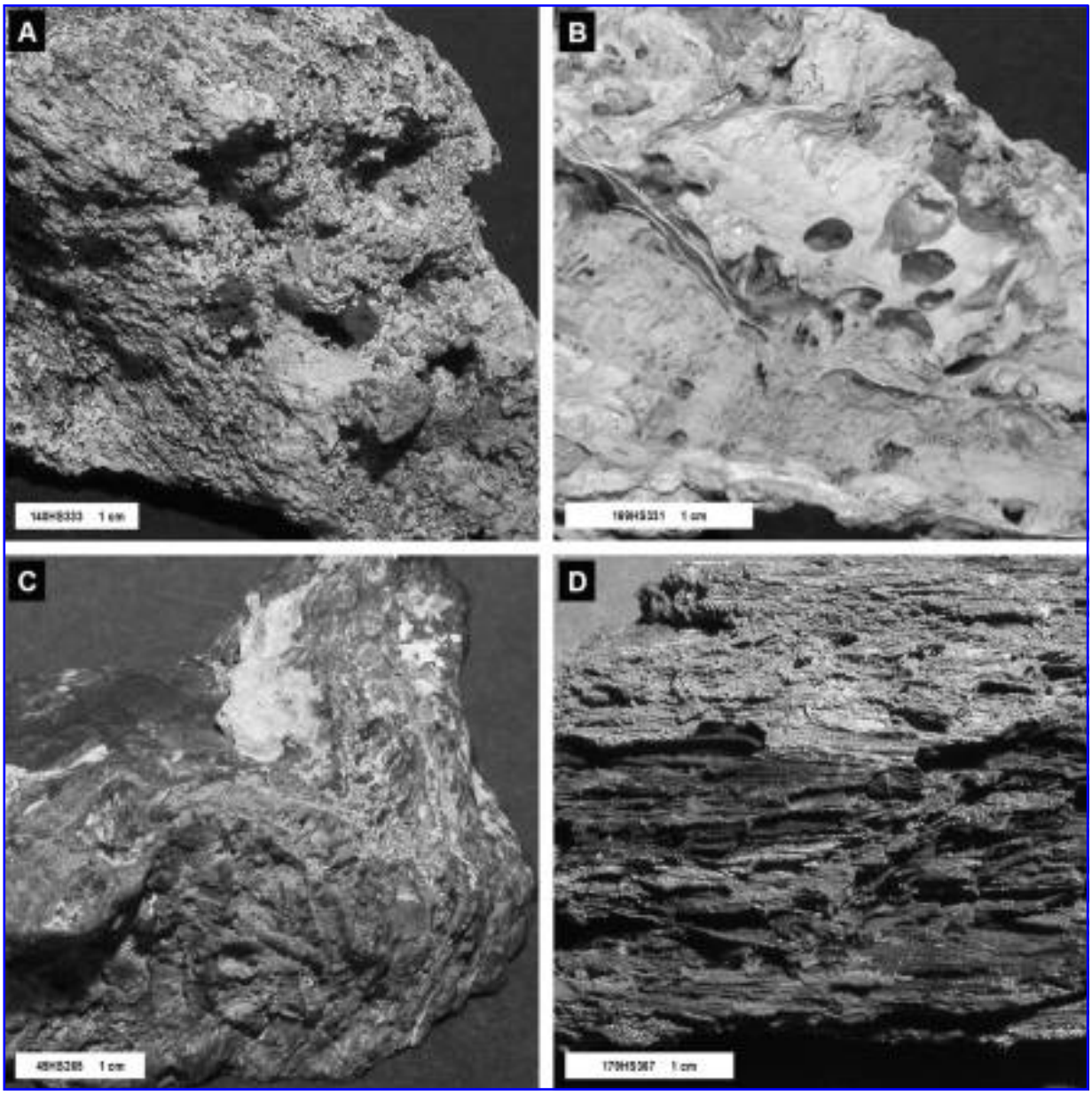

FIG. 1. Study samples exhibiting filamentous morphological biosignatures. (**A**) Freshwater limestone with calcite/dolomite-encrusted tubes over cyanobacterial substrates, Hainsfarth, Ries Crater, Germany (140HS333). (**B**) Opaline sinter replacing microbial mat exhibiting preserved filamentous fabric in voids, Hillside Springs, Yellowstone Park, USA (169HS331). (**C**) Hydrothermal vein sample with Fe-encrusted filaments preserved in chalcedony, Cady Mountains, California, USA (45HS265). (**D**) Goethite developed over filamentous fabric within oxidation zone of sulfide ore deposit, Cerro de Pasco, Peru (179HS367). Image credits: PAFSnet.

Chalcedony, Cady Mountains, California, USA (45)

The Lower Miocene volcanic and sedimentary sequence of the Sleeping Beauty Ridge region of the Cady Mountains (34°46′N, 116°17′W) has been extensively studied (Glazner, 1988). The volcanics are a well-known source of various types of agate and jasper (Henry, 1957).

Veining within the dacites and basalts extends to over 2 km and is up to 50 cm thick. Veins that contain subsurface filamentous fabric are mainly composed of chalcedony, Fe-hydroxides, and calcite, and are strongly enriched in trace elements Sb, As, Mo, Pb, Be, and Ag. The study specimens were collected by one of us (Hofmann) from a well-preserved silica-rich vein within weathered volcanic country rock (Hofmann and Farmer, 2000).

The filaments were formed within a hydrothermal regime a few hundred meters below the palaeosurface. The filament-bearing zones were originally porous and served by nutrient-rich fluids that provided a suitable subterranean habitat. Late-stage infilling of these voids with chalcedony and calcite preserved the filaments. The oldest filamentous fabric is heavily Fe-encrusted and macroscopically preserved, but no individual filament details are discernible (Fig. 1c and in Hofmann *et al*., 2002). Subsequent generations of filaments exhibit less Fe-cementation and show preserved individual morphology, including visible cores. The sub-micron size of these individuals prohibits detection within this study.

Goethite, Cerro de Pasco, Peru (179)

The Matagente ore body is part of the magmatic-hydrothermal Zn-Pb-Ag-Bi-(Cu) ore complex of Cerro de Pasco, which is situated 170 km NNE of Lima (10°38.5′S, 76°10.5′W). Prior to exploitation, the maximum extent of the ore body was 480 m × 200 m. Mining of the Pb-Ag deposit took place predominantly within the oxidation zone (Sangameshwar and Barnes, 1983), which reached approximately 100 m depth.

Oxidation zones of sulfide ore bodies commonly contain filamentous fabrics that were originally formed below a paleosurface (Hofmann and Farmer, 2000). Such an environment provides an energy source (usually from pyrite) for chemosynthetic organisms (Melchiorre and Williams, 2001). These (Fe-hydroxide) filamentous fabrics potentially act as substrates for subsequent growth of oxidation-zone minerals.

The study specimens were originally collected in 1955 by G. Christian Amstutz, a mine geologist at Cerro de Pasco. Externally, they exhibit a macroscopic, linear (fibrous) texture that is similar in appearance to "fossilized wood" (Fig. 1d) and has a high porosity (>50%). Iron hydroxides drape the surface in curtain-like laminae approximately 1 mm to 3 mm thick. Scanning electron microscopy observation shows that individual filaments are also preserved with core diameters of about 0.3 μm, though they are too small for observation with the instrumentation used in this investigation.

Endoliths

Specimens that contain endolithic microbial colonies were obtained from the extreme environments of 2 high-latitude sites on Earth [McMurdo Dry Valleys, Antarctica (Friedmann, 1982) and Haughton Crater, Devon Island, Canada (Cockell *et al*., 2002)]. Examples of both cryptoendoliths (microbes thriving within the intergranular fabric of rocks) and chasmoliths (microbes exploiting existing fractures and voids) were included. The specimens' host mineralogies range from quartz (orthoquartzite) to dolomite (marble) to gypsum (*var*. selenite). Examples of endoliths in other rock types are being sourced for future studies (Cockell *et al*., 2002; Jorge Villar *et al*., 2003).

Orthoquartzite, McMurdo, Victoria Land, Antarctica (114)

The dry valleys of Southern Victoria Land, Antarctica, extend across an area of 5000 km^2 and lie between 76°30′S and 78°30′S and 160°E and 164°E. Geomorphologically, they are a system of gouged glacial valleys with a predominant east-west trend. During the summer, air temperatures range between −15°C and 0°C, and can fall to almost −60°C in the winter. Less than 10 mm water equivalent of precipitation occurs annually. The Upper Devonian orthoquartzites of the Beacon Sandstone Formation outcrop throughout the dry valleys and contain well-studied examples of cryptoendolithic lichens and micro-algal communities (Friedmann, 1982; Friedmann *et al*., 1988; Siebert *et al*., 1996).

Specimens of exfoliated orthoquartzite that contain cryptoendoliths were collected by the British Antarctic Survey in 1995 from the Ross Desert McMurdo Dry Valleys at Linnaeus Terrace (77°36′S, 161°05′E elevation 1600 m). Much research has already been done on these and other rocks of the region (Friedmann, 1982; Wierzchos *et al*., 2003; Blackhurst *et al*., 2005), including analysis by way of techniques we employ here (Edwards *et al*., 1997, 2004). As such, these specimens provide an appropriate benchmark from which to draw comparison with other types of endolithic biosignature.

The rocks are colonized by photosynthesizing cryptoendolithic lichens that form by symbiotic association between unicellular green algae (phycobionts) and filamentous fungi (mycobionts). The physical characteristics of the fresh orthoquartzite (translucency and porosity) provide a favorable protective environment for these organisms. The outer surface is case hardened (indurated) and oxidized (though the brown coloration belies the low bulk iron content). Over

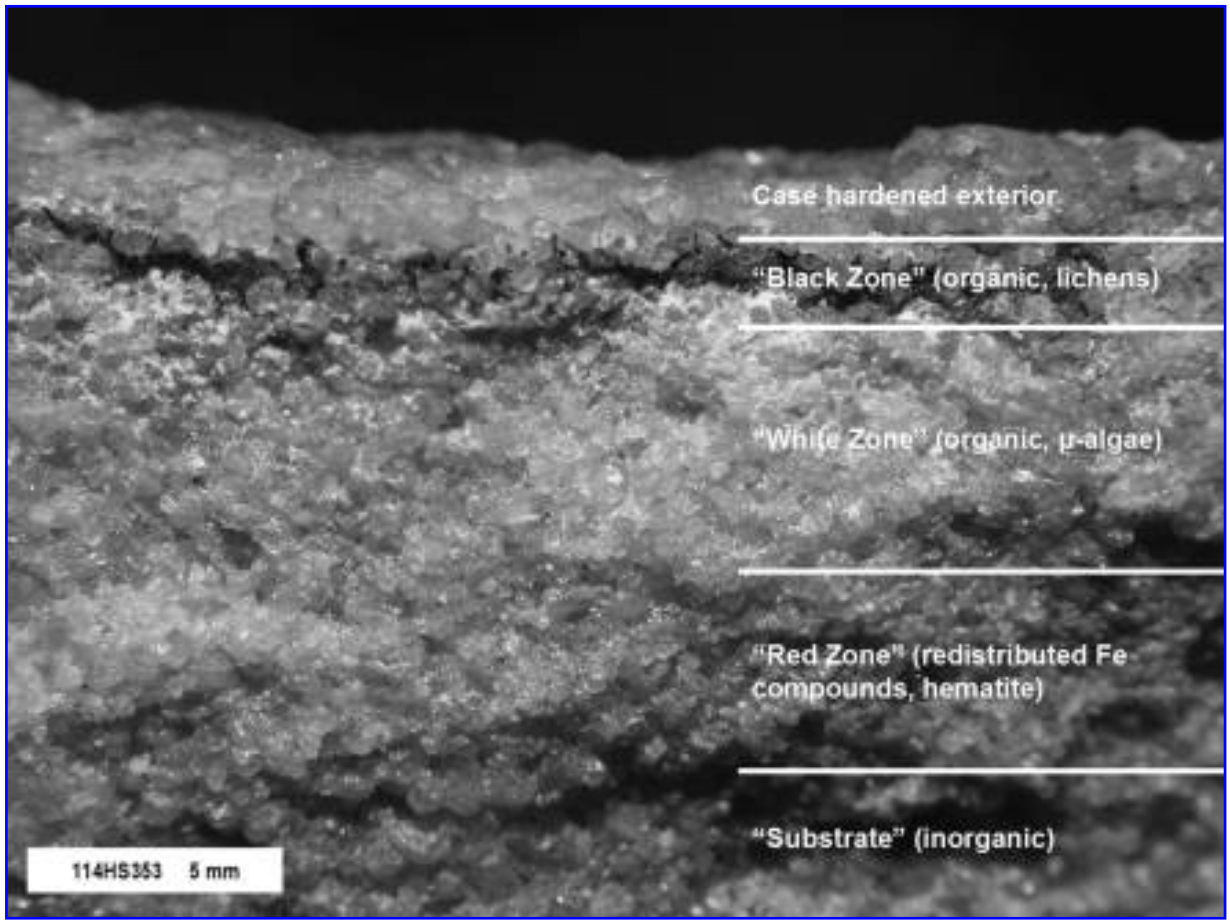

FIG. 2. Cryptoendolithic zonation in Beacon Sandstone (orthoquartzite), McMurdo Dry Valleys, Antarctica (114HS353) (after Friedmann, 1982). Way up is up. Image credit: PAFSnet.

time, oxalic acid secretions from the lichens dissolve the intergranular cement of the host rock, which leads to bioweathering and exfoliation of the rock surface (Sun and Friedmann, 1999).

Communities typically occur as distinct layers within the rock fabric (Friedmann *et al*., 1988). Figures 2 and 17c show the sequence in one of the study samples. The upper (near surface) black band is commonly 1 mm thick and close to the exfoliation interface. The coloration is due to UV protective pigments, such as scytonemin, which is produced by these organisms. Below this layer is a white zone of between 1 mm and 4 mm thick, where the lichens have mobilized iron compounds and leached the rock of iron-bearing minerals (Sun and Friedmann, 1999), concentrating them in a red zone at the base of the white zone. A green algal layer is typically found below these zones. Growth and development of these cryptoendolithic communities is extremely slow.

Marble, McMurdo, Victoria Land, Antarctica (194)

In other parts of the McMurdo Dry Valley system, crystalline rocks host examples of chasmolithic cyanobacteria (Jorge Villar *et al*., 2003). Some specimens were collected by the late David Wynn-Williams (British Antarctic Survey) during a field campaign from a talus slope in the vicinity of the Long Term Ecological Research site on Andrews Ridge near Lake Hoare, Taylor Valley (77°38′S, 162°52′S). Our study sample (194HS435) is a weathered marble colonized by *Chroococcidiopsis*, a desiccation-resistant, radiation-resistant cyanobacterium (Erokhina *et al*., 2002).

The "fresh" marble is almost white and has a crystalline fabric (Fig. 3a). Microbial growth occurs along fracture planes on both fresh and internal weathered surfaces, which suggests chasmolithic behavior. Colonies are readily distinguishable

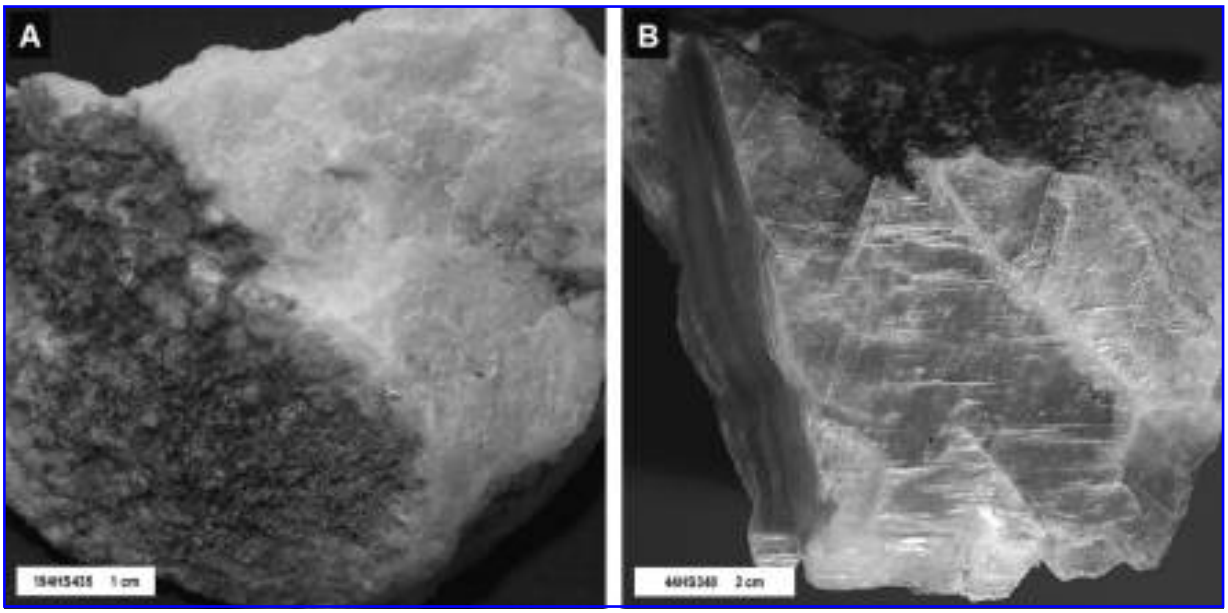

FIG. 3. Examples of chasmolithic colonization in carbonate and laminated sulfate rocks. (**A**) Marble, McMurdo Dry Valleys, Antarctica (194HS435). (**B**) Gypsum (*var.* selenite), Haughton Crater, Devon Island, Canada (44HS340). Image credits: PAFSnet.

from the white marble due to their coloration (blue-green) and penetrate deep (~1 cm) into the rock (Fig. 20b). We include this sample in our inventory of morphological biosignatures on the basis of (a) crystalline fabric, (b) biofluorescent properties (Fig. 21), and (c) comparison with cryptoendolithic samples from the same region (114).

Gypsum, Haughton Crater, Devon Island, Canada (44)

The Haughton impact structure is located in the western region of Devon Island in the Canadian High Arctic (75°22′N, 89°41′W) and was formed during the late Eocene (~39 Ma) (Sherlock *et al*., 2005). Surface mapping and the local gravity signature confirm a crater of approximately 24 km in diameter (Grieve, 1988; Pohl *et al*., 1988; Scott and Hajnal, 1988). The impacting asteroid (or comet) penetrated target rocks comprised of a thick carbonate sequence (~1.8 km) that is underlain by Precambrian granites and gneisses. Allochthonous polymict impact breccia dominates the central portion of the crater (~10 km diameter), which is largely made up of target rock clasts from the carbonate sequence plus basement gneisses. Evidence for impact-induced hydrothermal activity is well preserved within the structure, including sulfate mineralization and mobilization (Osinski and Spray, 2003). Microbial colonization within these sulfate deposits has recently been described (Parnell *et al*., 2004).

Specimens of microbe-bearing gypsum were collected by one of us (Parnell) from sites within the impact breccia unit adjacent to the Paleozoic basement sediments. The gypsum is in the form of selenite, which is highly pure with large transparent cleavage folia (Figs. 3b and 23b) (Osinski and Spray, 2003). The microbes inhabit the interlaminar space between crystals and appear up to a few centimeters from the external margins. The clarity of the selenite crystals provides a "window" through which to observe the microbial communities at successive levels. Two species of cyanobacteria have been identified, *Gloeocapsa alpine* (Naegeli) Brand and *Nostoc commune* Vaucher (Parnell *et al*., 2004). Given the nature of their host, these photosynthesizing chasmoliths are salt tolerant and have been shown to be dependent on photo-protective pigment synthesis (Edwards *et al*., 2005a).

Experimental

All imaging, analytical, and geotechnical activities were performed within standard open laboratory conditions. Although designed for use on Mars, the instruments and tools from the Beagle 2 PAW [with the exception of the Flight Spare

XRS (FS-XRS)] could be used under these circumstances without significant degradation in performance. Each device was removed from the PAW (Fig. 5 in Pullan *et al*., 2003) and operated in stand-alone mode.

Even though all samples were imaged, some could not be analyzed by all methods due to either paucity of material available for destructive analysis or nonavailability of some of the instrumentation. As this study is part of an ongoing program, it was considered undesirable to commit to the rock crusher unique specimens that display visual features of interest. Nevertheless, a subset of the study samples benefited from the complete array of techniques.

Ultimately, one would systematically analyze, in the field (*i.e*., at the planetary surface), and interpret the collective data at each scale by proceeding from coarse (far from target) to fine (close to or in contact with target). For the purposes of this study and to avoid the inevitable "miss hit," the reverse was adopted, at least initially, to enable the relatively small microbial relict features to lie within a field of view at each scale (if this was achievable). Where possible, both weathered and fresh examples of each sample were compared; and, in some cases, sawn (unpolished) surfaces were also investigated. Thus, external surfaces (pre-splitting), internal surfaces (post-splitting), and prepared surfaces (post-grinding) were represented. Instrument positioning with respect to sample targets (*i.e*., emulating robotic placement) was achieved manually by way of simple retort stands, clamps, mechanical stages, and tripods.

Since the identification of morphological biosignatures is the dominant theme of this investigation, spatial imaging is the obvious primary technique. In the framework of this paper, and planetary fieldwork in general, analytical data provide essential context with which to constrain interpretation of the images, and geotechnics provide the means by which to access the features.

Imaging

Imaging was performed at 3 working distances between the observer and the target: proximal (~100 cm), macroscopic (~10 cm), and microscopic (~1 cm). We consider this range to be synonymous with the immediate radial "working zone" of a terrestrial field geologist who is suitably equipped with tools of the trade (hammer, field lens, portable analyzers, samplers, etc.), and we adopt the terms proximal, macroscopic, and microscopic to differentiate from activities beyond the physical reach of the observer (*i.e*., "remote" sensing) that require effort (mobility) to reach. Our use of the term *proximal* would naturally fit within the lower bounds of the microfacies scale (m to cm size targets) described by Cady *et al*. (2003). In the planetary context, our analogy applies equally to static planetary landers or stationed mobile vehicles equipped with robotically deployed scientific payloads (Golombek, 1997; Pullan *et al*., 2003; Squyres *et al*., 2003; Vago *et al*., 2003; Baglioni, 2003).

Dark enclosures, translation stages, and controlled illumination were specially constructed and utilized for all the imaging work (Fig. 4). Both Beagle 2 cameras (stereo camera and microscope) also benefited from reduced ambient room temperatures achieved in the laboratory to minimize noise.

Proximal and macroscopic imaging

The Beagle 2 Development Model (DM) stereo camera was used for both proximal imaging (at 600 mm range using the geology filter set[†]) and macroscopic imaging (at 80 mm range using the ×6.4 close-up lens filter) (Griffiths *et al*., 2005). The DM camera has a spatial resolution of 50 μm pixel^{-1}. Square "working" FOV of 26 cm × 26 cm and 4 cm × 4 cm, respectively, were achieved by cropping all images to negate the slight fall-off in CCD flat-field response observed at the peripheral regions in the DM camera. In macroscopic mode, the DM camera has similar capabilities to the Microscopic Imager on the Mars Exploration Rovers (31 mm × 31 mm FOV at 30 μm pixel^{-1}).

Spectral imaging was possible at room temperature (18°C) with all filters with the exception of 440 nm (blue) due to its low (80%) transmission characteristics. Illumination was provided by a 4700 K daylight halogen lamp for proximal (spectral) imaging and RGB dichroic additive filtered light via a cold ring-light system for macro-

[†]On Beagle 2 the geology filter set was shared between the 2 cameras of the Stereo Camera System. For our laboratory experiments a spare filter wheel was populated with 11 geology filters plus the close-up lens. The ideal center wavelengths of the geology filters are (expressed in nm) 440, 530, 600, 670, 750, 800, 860, 900, 930, 965, and 1000. The 480 nm filter could not be accommodated. The characteristics of all filters are specified in Griffiths *et al*., 2005.

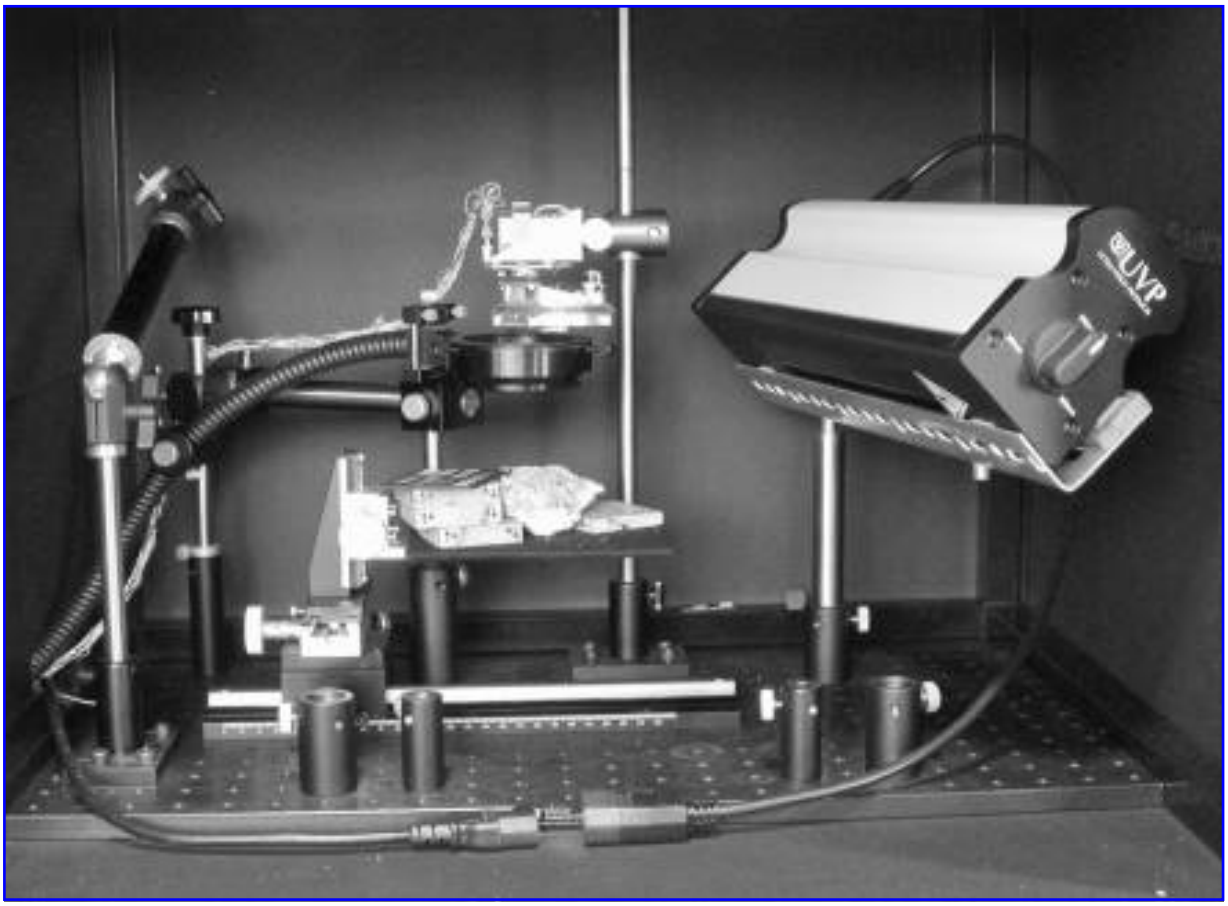

FIG. 4. Experimental setup for macroscopic imaging. The Beagle 2 DM camera (top center) was positioned approximately 10 cm above the sample (center). A cold ring light provided controlled illumination from a light source outside the enclosure (see text). The sample could be moved vertically (for focusing) and horizontally (for fine positioning and stereo imaging) using a triaxial stage. The UV lamp (right) was used for fluorescence work. Proximal imaging involved positioning the camera higher (~60 cm), removing the ring light and illuminating the scene with a daylight lamp (see text). Image credit: PAFSnet.

scopic work. Single camera stereoscopy (using lateral displacement) and UV fluorescence (using off-axis UVA/UVB/UVC 8W sources) were also features of macroscopic imaging with the use of the DM camera. In the case of the latter, initial experiments with samples of fossilized amber (178HS369) and fluorite (184HS379) confirmed the usefulness of UV illumination for macroscopy. All DM camera images were calibrated to level 2 (bias and dark current) and occasionally to level 3 (level 2 plus flat field), where this was deemed appropriate (low albedo surfaces).

Multi-spectral imaging was performed with a CRI Inc. Nuance system provided by Newport LOT-Oriel and equipped with a standard Nikon 60 mm macro lens. The Nuance system is based on a stack of Lyot liquid crystal filters placed in front of a 1.3 Mpixel scientific grade CCD. Each filter can be "tuned" by applying an appropriate electric field, which thus alters the overall transmission characteristics of the stack. For our experiments, LOT-Oriel provided a Nuance system with a wavelength range of 420 nm to 720 nm with 10 nm pass-band interval. The system is controlled via a supplied software interface.

Microscopic imaging

The Beagle 2 microscope is a fixed-focus monochromatic camera with integral illumination LEDs for color (RGB) and UVA (373 nm) imaging (Thomas *et al*., 2004). Focusing is achieved by mechanically translating the entire microscope incrementally along its optical axis (Pullan *et al*., 2003) and combining all the in-focus elements of each image, acquired at each position, into a sin-

gle image. As a consequence, depth information is also obtained. At a nominal standoff distance of 12 mm (range 9 mm to 15 mm ±3 mm), the FOV is 4.1 mm × 4.1 mm (naturally square due to optics/CCD arrangement). This equates to a scale of 4 μm pixel^{-1}.

For microscopic imaging, the sample was secured, and the microscope moved relative to it at increments of 40 μm (equivalent to the depth of field). This was achieved with a commercial precision-motorized vertical stage and control software, which emulates operation at the planetary surface (Pullan *et al*., 2003). Samples with high relief at this scale required up to 160 individual images for color/UV compositing. All images were calibrated to level 4 (bias, dark current, flat field, and alignment). No image cropping was necessary since the microscope used in this study [Qualification Model (QM)] was fully calibrated.

Analytical

X-ray fluorescence (XRF). The Beagle 2 FS-XRS was not considered appropriate for this study, since the system relies on passive cooling and is, therefore, confined to an environmental chamber. A variant of the XRS (using commercial electronics connected to a Beagle 2 type Detector Head Assembly) was available but not used. In place of the FS-XRS, we employed a TN Technologies Spectrace 9000 commercial energy-dispersive XRF spectrometer designed for field use, which utilizes the same excitation method as the Beagle 2 system (^{55}Fe and ^{109}Cd) plus ^{241}Am (Ramsey *et al.*, 1995). The TN9000 is designed for terrestrial applications and uses an HgI_2 detector (resolution 260 eV at Mn-Kα). The XRS is designed specifically for Mars and uses a Si PIN diode detector (resolution 390 eV Mn-Kα for the FS-XRS and 340 eV for the flight model XRS). The analytical performance of the FS-XRS has been compared with the TN9000 (Talboys, 2006), which therefore justified the use of the latter in this study.

The TN9000 was configured vertically with the ~25 mm window (similar in footprint to the Beagle 2 XRS) facing upward. Samples were presented face down over this aperture for the duration of the measurements. Useful elements determined with this spectrometer include K, Ca, Ti, Mn, Fe, Sr, Zr, Mo, Pb, Rb, and Ba, plus Cu, Ni, Zn, and As if these are present in relative abundance (>100 ppm). This is similar to the capability of the Beagle XRS (Talboys, 2006).

Bulk geochemistry was determined by laboratory wavelength dispersive XRF (WDXRF) in order to set a benchmark of elemental concentrations prior to the field measurements and satisfy a broader elemental range expected of future instruments. Standard methods for determination of major elements (fusion beads) and trace elements (pressed powder pellets) were used for those samples with sufficient residual material available. All *in situ* data were corrected for instrumental bias with geochemical standards.

X-ray diffraction (XRD). X-ray diffraction data were recorded from small areas (< mm^2) of unprepared samples by way of an INEL 120° curved position-sensitive detector (PSD). This detector has an output array of 4096 digital channels, which represents an arc of 120° 2θ and permits the simultaneous measurement of diffracted X-ray intensities at all angles of 2θ across 120° with a static beam-sample-detector geometry (Fig. 5).

A Microsource® was employed to generate high brightness Cu-Kα radiation with the source operating at 40 kV (2 mA). Horizontal and vertical slits were used to restrict the beam to a chosen size appropriate to the dimensions of the micro area selected on the solid sample; the micro area on the sample was viewed with a CCD image-capture system, and the whole sample was manipulated (spun) by a triaxial stage. The limited focus depth of field of the optical system was used to bring the sample to the correct height to be intercepted by the X-ray beam, whose position was predetermined by way of a fluorescent screen with a fiducial mark in focus at the point where the beam was also in focus on the screen. In this mode, micro-diffraction experiments were performed *in situ*, without destructive sampling.

Measurements were made in reflection geometry with the sample surface at a slight angle to the incident beam. Data collection times were only a few minutes for each sample, and the angular range recorded was 4° to 120° 2θ. NIST silicon powder SRM640 was used as an external 2θ calibration standard.

Standard XRD was also performed on prepared powders using a Philips PW1710 diffractometer. A long fine-focus X-ray tube was used to generate Cu-Kα radiation at 40 kV (30 mA) and fitted with a Ni filter. A step size of 0.02° 2θ was used over a scan range of 4° to 64° 2θ at 1° 2θ min^{-1}.

Depending on the sample acquisition and processing capability of future missions, it may be that *in situ* XRD will be performed on well-ho-

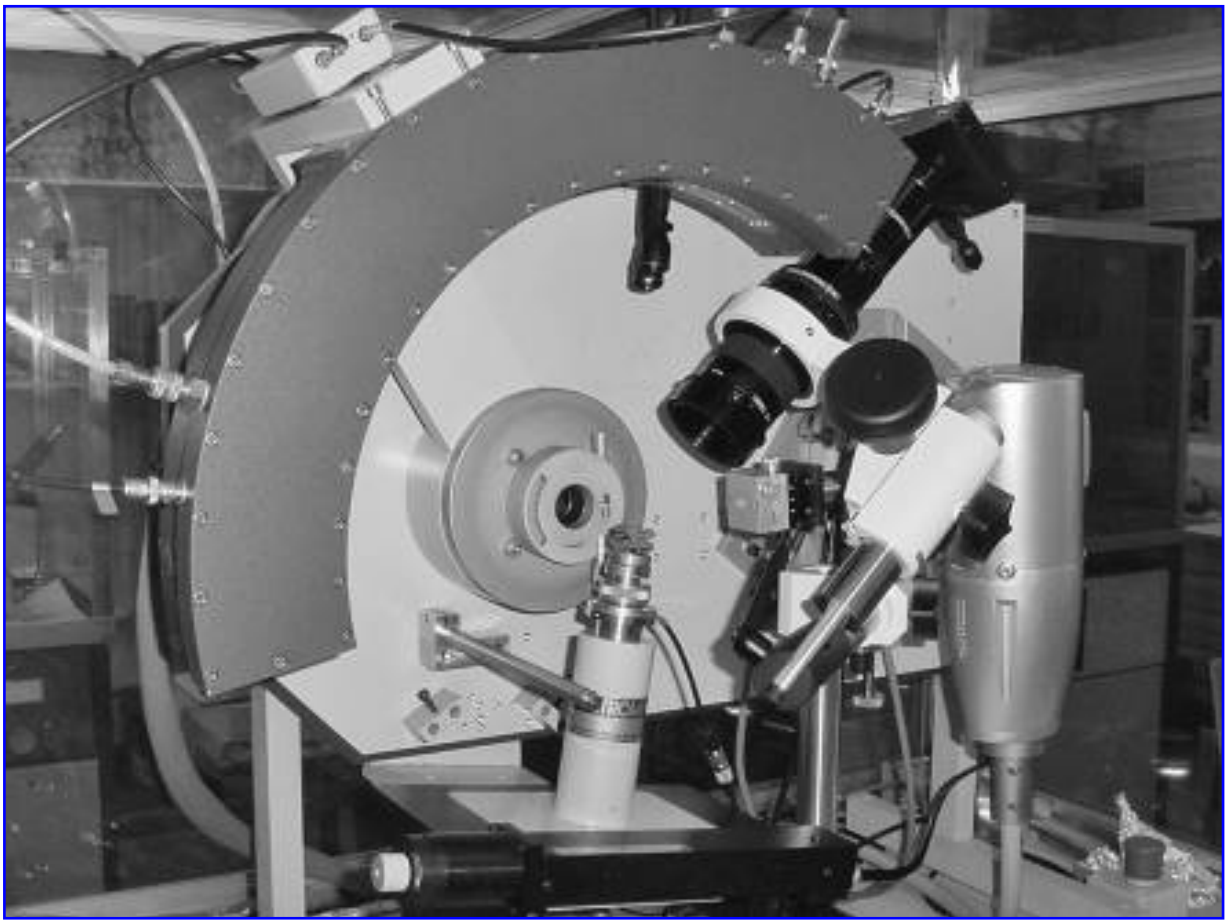

FIG. 5. Laboratory X-ray diffractometer used for *in situ* analysis of natural (unprepared) specimens. Thumbnail-sized samples were secured on a spinning triaxial stage (foreground center). High brightness Cu-Kα radiation was generated by a Microsource® (right) and the beam restricted to a micro area ($<mm^2$) on the target sample (see Fig. 10). A CCD camera (top right) images the same micro area. The curved PSD (top left) has an arc of 120° 2θ for simultaneous measurement across the range. Image credit: Department of Mineralogy, Natural History Museum, London.

mogenized bulk powder (ideal), partially sorted crushate, or individual monomineralic clasts (due to limited sample volume). This system, therefore, represents an on-board laboratory instrument that is fed coarse powder or crushate, as might be the case for ExoMars, though the operating principle is not intended to emulate the actual instrument.

Raman spectroscopy. Raman spectroscopy has long been advocated as a technique for *in situ* planetary exploration (Israel *et al.*, 1997; Wynn-Williams and Edwards, 2000; Tarcea *et al.*, 2002; Ellery and Wynn-Williams, 2003; Sharma *et al.*, 2003; Wang *et al.*, 2003; Edwards *et al.*, 2005b). A Bruker IFS66 IR spectrometer with FRA 106 Raman module and an Nd3+/YAG laser operating at 1064 nm was used in conjunction with a Raman nonconfocal microscope fitted with a ×40 objective. This configuration provided a sample footprint of approximately 20 μm diameter. Spectra were recorded between 50 and 3500 cm^{-1} in increments of 4 cm^{-1}. In addition, a Renishaw *In-Via* confocal Raman microscope operating at 514 nm and 785 nm was used with a ×50 objective, which results in a smaller target footprint of 2 μm diameter. Typical laser power ranged between 0.5 mW and 50 mW.

Mössbauer spectroscopy. Iron is abundant at the surface of Mars (Knudsen, 1989; Knudsen *et al.*, 1990, 1992; Rieder *et al.*, 1997). In recent years, Mössbauer spectroscopy has contributed much to our understanding of the properties of martian rocks and soils (Morris *et al.*, 2004, 2006; Klingelhöfer *et al.*, 2004) and has been cited as a useful tool for *in situ* astrobiology (Wilson, 1999; Schröder *et al.*, 2005).

The Beagle 2 QM Mössbauer spectrometer (Klingelhöfer *et al.*, 2003) was used to determine Fe-bearing mineralogy and Fe oxidation states for most of the study samples. The instrument has 512 data channels, operates in backscatter geometry with a triangular waveform at a drive frequency of ~24 Hz and a standard (but selectable) calibrated velocity range of ± 12 mm s^{-1} and has a primary ^{57}Co gamma radiation source. If a flat surface below the contact plate is assumed, the target area illuminated by the incident 14.4 keV ^{57}Co gamma radiation has a diameter of ~1.4 cm. The sampling depth in basaltic materials is ~0.03 g cm^{-2}, or ~3 mm in air-fall dust and ~0.2 mm for coherent rock (Klingelhöfer *et al.*, 2003). The instrument is based at the University of Mainz, Germany, where it has been used extensively to support the NASA Mars Exploration Rover mission since 2003 (Schröder *et al.*, 2004).

Many of the study samples are depleted in (or devoid of) Fe-bearing minerals (Table 1). However, flight heritage, synergy with other techniques such as XRF/XRD, and consistency within our overall program make it important to include the Mössbauer technique. As will be seen, samples that appear visually and spectrally oxidized, yet yield null Mössbauer spectra, can benefit from measurement.

Geotechnics. Due to the paucity of material available for destructive testing, no *in situ* sample preparation method was employed as an integrated part of this study. However, it is worth mentioning geotechnics in the context of our work. Tools provide a means of sample acquisition (Richter *et al.*, 2002; Pullan *et al.*, 2003) and surface preparation (Gorevan *et al.*, 2003b). Apart from these primary functions, physical property data can help identify rocks and soils and determine preservation state (Richter *et al.*, 2002; Arvidson *et al.*, 2004a, 2004b). Grinders and samplers are inherently destructive devices that would likely destroy any morphological biosignature preserved as an endolith or relict structure inside a rock. Splitting a rock with a hammer, a tried and tested technique used by every field geologist, is more appropriate for our study.

Ideally, geotechnical elements of a payload would consist of a hammer, a grinder, and a rock/soil sampler or some device that is capable of performing all these functions. For this study, we assume this is the case, and targets are presented in formats that would be available to the field geologist (*i.e.*, external weathered surfaces through to internal fresh surfaces). By way of justification, we introduce some early development results from our experiments with the Beagle 2 QM PLUTO as a rock splitter (Fig. 6).

RESULTS

Imaging data from our experiments on the study samples are described in the following sections and presented in Figs. 7–9, 13, 14, 16–18, 20, 21, and 23. Proximal images are naturally low resolution due to a combination of sample/feature size and the limited spatial capabilities of current space camera technology. This, however, is not an issue for macroscopic and microscopic imaging.

Analytical data are summarized in Tables 2 through 5, and related geotechnical work is presented in Fig. 6. For this paper, we utilize the analytical data to support the imaging results. Raman spectroscopy results are presented in more detail in a companion paper (Edwards *et al.*, 2007), but key observations made during this study are also presented in Table 4.

The interpretations that follow are based on the experimental *in situ* data only and therefore do not formulate a complete characterization of each sample. An evaluation of the ability to determine biogenicity and thereby justify sampling operations, based on these specific *in situ* measurements, is presented for each sample studied.

Microbial filaments

Samples that exhibit filamentous fabric (140, 169, 45, and 179) generally present high relief at macroscopic and microscopic scales. The open fabric exhibited by all the study samples proved advantageous for 3-D imaging with the use of stereo techniques and incremental focusing. Multi-spectral imaging was particularly useful, especially where mineralogical spectral signatures coincided with morphology (*i.e.*, 140HS332). These signatures were also corroborated by selective *in situ* analysis by XRD and Raman.

Freshwater limestone, Hainsfarth, Ries Crater, Germany (140)

Proximal imaging of samples 140HS332 and 140HS420 with the Beagle 2 DM camera (Fig. 7) differentiated external surfaces (sintered) from internal surfaces (exposed tubes) on the basis of

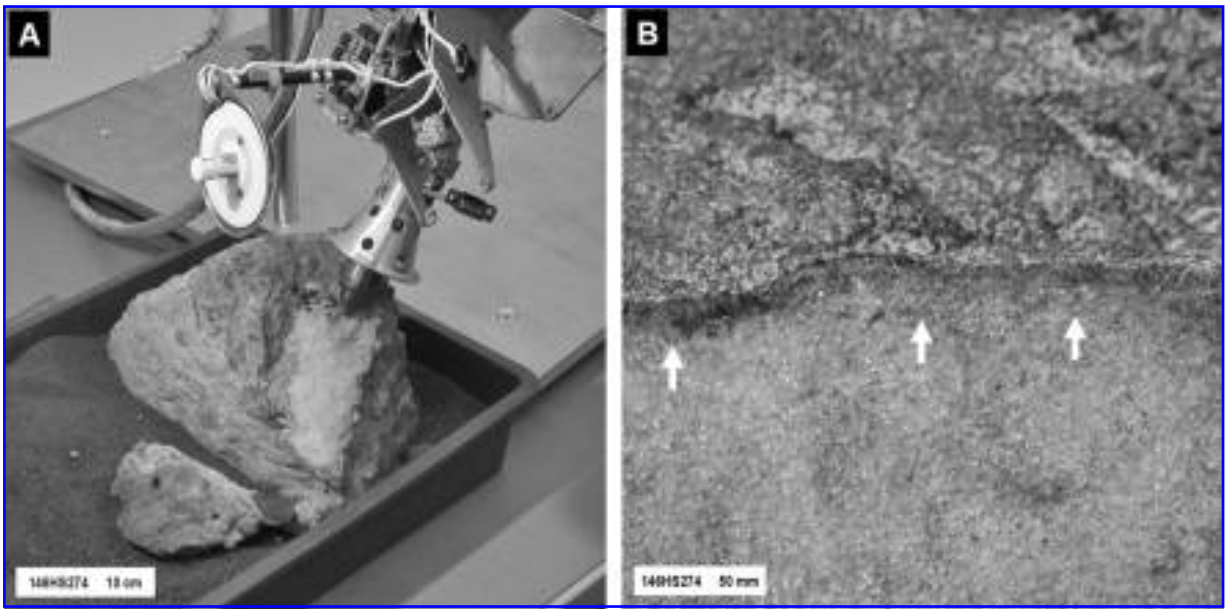

FIG. 6. ***In situ*** **rock splitting and sample preparation.** (**A**) The soil sampling "Mole" from Beagle 2 being used to split a sample from 146HS274 (orthoquartzite, Montana, USA). This material has similar physical properties to Beacon Sandstone from Antarctica (114HS353, see text). (**B**) Close-up view of the spalled fragment showing microbial colonization (cryptoendoliths) at the interface between the weathered exterior (upper part of image) and "fresh" interior (lower part of image). Instrumentation: Beagle 2 QM PLUTO. Image credits: PAFSnet.

texture, overall reflectance (albedo), coloration (due to iron staining), and spectral signature (Fig. 8).

Proximal camera observations reveal a heterogeneous texture that consists of a basically fibrous framework that shows preferred lineation, which, in some areas, appears to be coated by a smooth surface film (Fig. 7a). Macroscopy provided further details of the fibrous fabric and documented the delicate aligned, open texture (Fig. 7b), which consists of intertwining filaments that present a partially matted appearance. Cross-sectional views of the filaments indicate that they are hollow, and this is clearly confirmed by the microscope images in which the filaments appear as tubes in both longitudinal and cross section (Fig. 9). Inner tube diameters are commonly ~40 μm. The tubes are defined by encrustations of a mineral nature with a regular thickness of about 40 μm. Specular reflections from fresh uncoated tubes suggest the presence of well-developed crystals <10 μm in size (Fig. 9a). Precipitates of another mineral with a lower albedo and different reflectance occur around the high albedo-mineral–encrusted filaments (Fig. 9b).

Multi-spectral macroscopic imaging with the Nuance system identified 2 distinct mineral signatures on fresh surfaces (Fig. 8). These were later confirmed as calcite and dolomite by both XRD (Table 3 and Fig. 10) and Raman spectroscopy (Table 4 and Fig. 11). Raman spectroscopy was able to distinguish the fine-scale distribution of dolomite within the outer portions of the mineralized filaments, as well as isolated occurrences of gypsum in the matrix (Table 4 and Fig. 11). Furthermore, opaque black spots (Fig. 9b) were confirmed to be organic carbon by Raman spectroscopy (Table 4); however, the spectral signature is broad, typical of degraded chemical species, so the compound could not be identified (Edwards *et al.*, 2007). Organics associated with the tubes themselves, either as integrated remnants or as residues on the inner walls, are absent. Raman also detected the presence of gypsum within the tube structures (Fig. 11). Mössbauer data confirm that the iron content of veneered surfaces is less than that observed on fresh surfaces, *i.e.*, tubes in cross section (Table 5 and Fig. 12).

Relatively high trace Sr levels were observed on both tube (806 ppm) and sintered (1118 ppm) surfaces.‡ The corresponding bulk value measured by WDXRF (2327 ppm) falls within the well-defined range (2140–2940 ppm) reported by Pache *et al.*, 2001.

‡Marine carbonates of Jurassic age (pre-impact) in the Ries area have lower Sr concentrations (<200 ppm) suggesting the Hainsfarth limestones were deposited in lake waters enriched in Sr^{2+} (Arp, 1995).

TABLE 2. *IN SITU* XRF DATA

Sample[a]	*TiO_2*	*Fe_2O_3*	*MnO*	*CaO*	*K_2O*	*As*	*Ba*	*Cu*	*Mo*	*Ni*	*Pb*	*Rb*	*Sr*	*Zn*	*Zr*
140: Limestone (tubes)	0.06	0.97	0.07	12.68	0.25	*36*	78	*0*	4	*97*	0	14	860	*37*	19
140: Limestone (sinter)	0.0	0.28	0.06	18.44	0.0	*44*	63	*28*	4	*51*	0	0	1118	116	8
169: Opaline sinter (exterior)	0.0	0.22	0.04	0.39	0.19	*44*	0	*38*	2	0	0	11	9	*82*	10
45: Chalcedony (interior, sawn)	0.0	20.59	0.12	1.04	0.06	443	43	129	40	0	132	13	45	186	5
179: Goethite (interior)[b]	0.0	34.79	0.09	0.0	0.0	656	0	1700	5480*	0	0*	646	24	*0*	13
179: Goethite (exterior, coated)[b]	0.0	34.15	0.13	0.04	0.03	1334	0	1000	6137*	0	0*	475	21	*0*	16
114: Orthoquartzite (interior)	0.03	0.02	0.0	0.09	0.06	*0*	13	*0*	4	0	15	0	8	*0*	44
114: Orthoquartzite (exterior)	0.02	0.23	0.0	0.19	0.04	*25*	0	*0*	0	0	0	0	14	*0*	37
194: Marble (interior)	0.0	0.05	0.0	14.90	0.08	*13*	0	*0*	0	0	0	0	30	*83*	0
194: Marble (exterior)	0.03	0.32	0.03	12.85	0.18	*0*	0	*33*	0	0	0	0	38	*92*	7
44: Selenite (cleavage surface)	0.0	0.0	0.0	17.62	0.0	*0*	0	*0*	3	0	14	6	246	*34*	0

Elemental data obtained using TN Spectrace 9000 portable XRF, courtesy Open University, UK. All surfaces natural unless otherwise stated.
Major elements expressed in weight percent (wt%) oxide and trace elements in ppm. All iron reported as ferric.
Other major elements including Si and Mg are not determined with the TN9000 instrument (see text).
Italicized data below reasonable limit (Phil Potts, Open University, personal communication).
[a]See text for descriptions.
[b]Values marked with a * are questionable (see text).

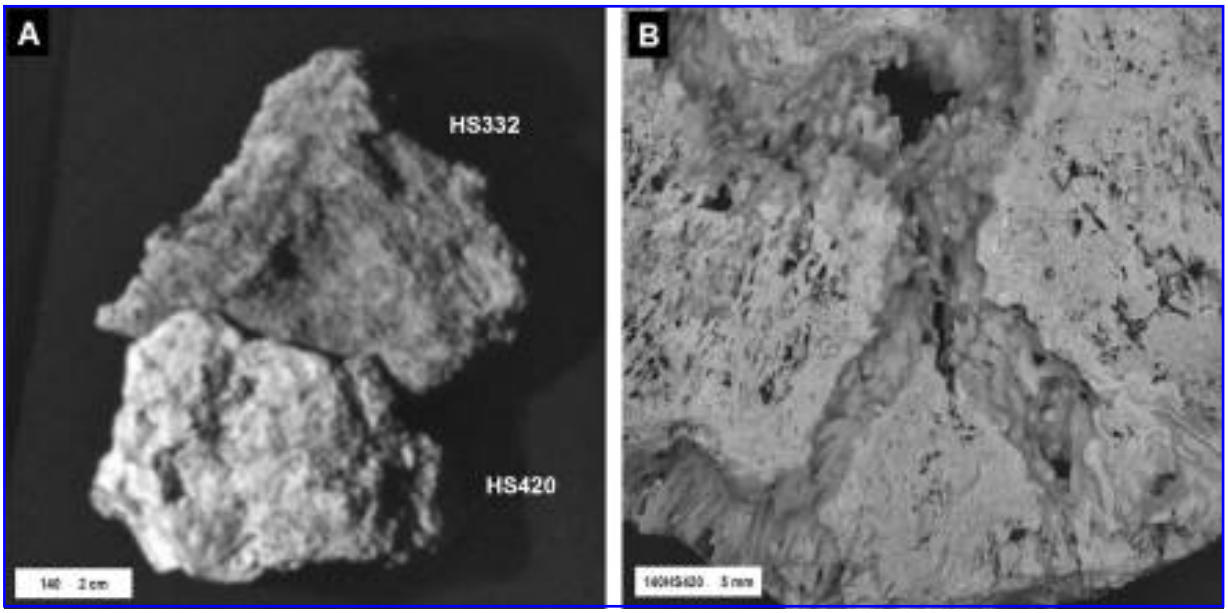

FIG. 7. Proximal and macroscopic imaging of freshwater limestone, Ries Crater, Germany (family ID 140). (**A**) Samples 140HS332 (upper: example of fresh interior) and 140H420 (lower: example of sintered exterior) as viewed at 60 cm with the 530 nm filter. (**B**) Macroscopic image of the external surface of 140HS420 showing sintered surface and associated heavily dolomitized tubes. Instrumentation: Beagle 2 DM stereo camera. Image credits: PAFSnet.

Biogenetic evaluation

These deposits formed in an impact crater lake, *i.e.*, a potentially habitable environment. The heterogeneous texture and fabric, along with the strongly aligned fibrous texture that is covered in places with a smooth film and the intertwined nature of the mineral-encrusted hollow tubes, point to a rock that could have had biogenic potential. The calcite composition of the filaments and the

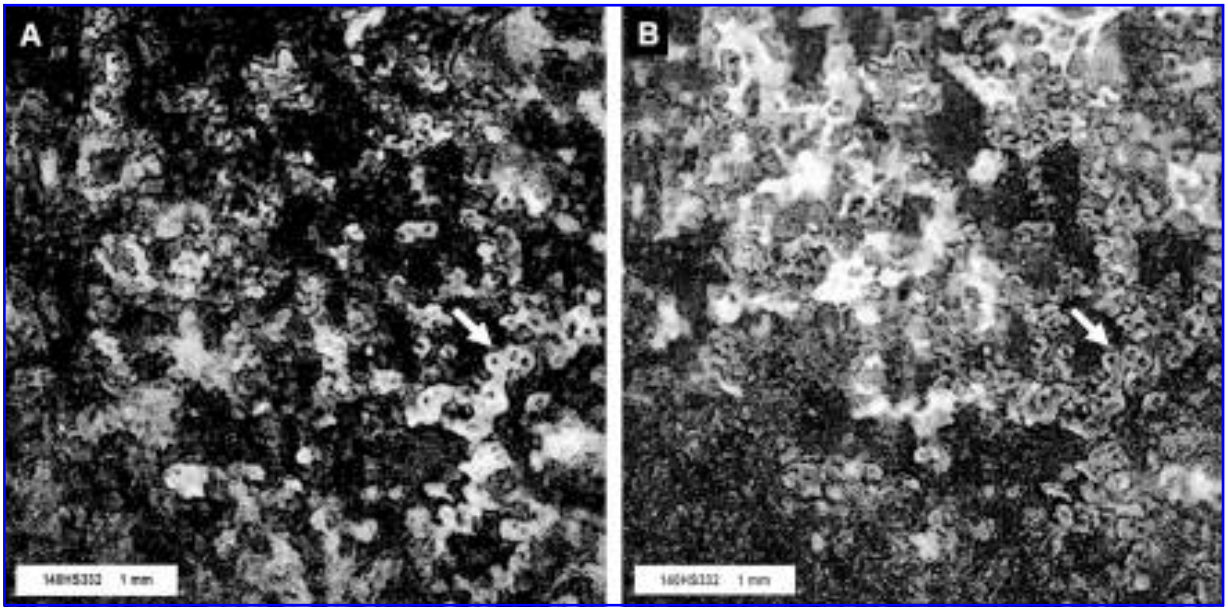

FIG. 8. *In situ* multi-spectral macroscopic imaging of sample 140HS332 (freshwater limestone, Ries Crater, Germany). Calcified tubes (**A**) and dolomitic matrix/veneered surfaces (**B**) can be discriminated due to subtle differences in spectral signature between 420 nm and 720 nm. Both images are the same FOV. Black areas common to (A) and (B) are in shadow (*i.e.*, no data). Instrumentation: Nuance camera system. Image credits: PAFSnet.

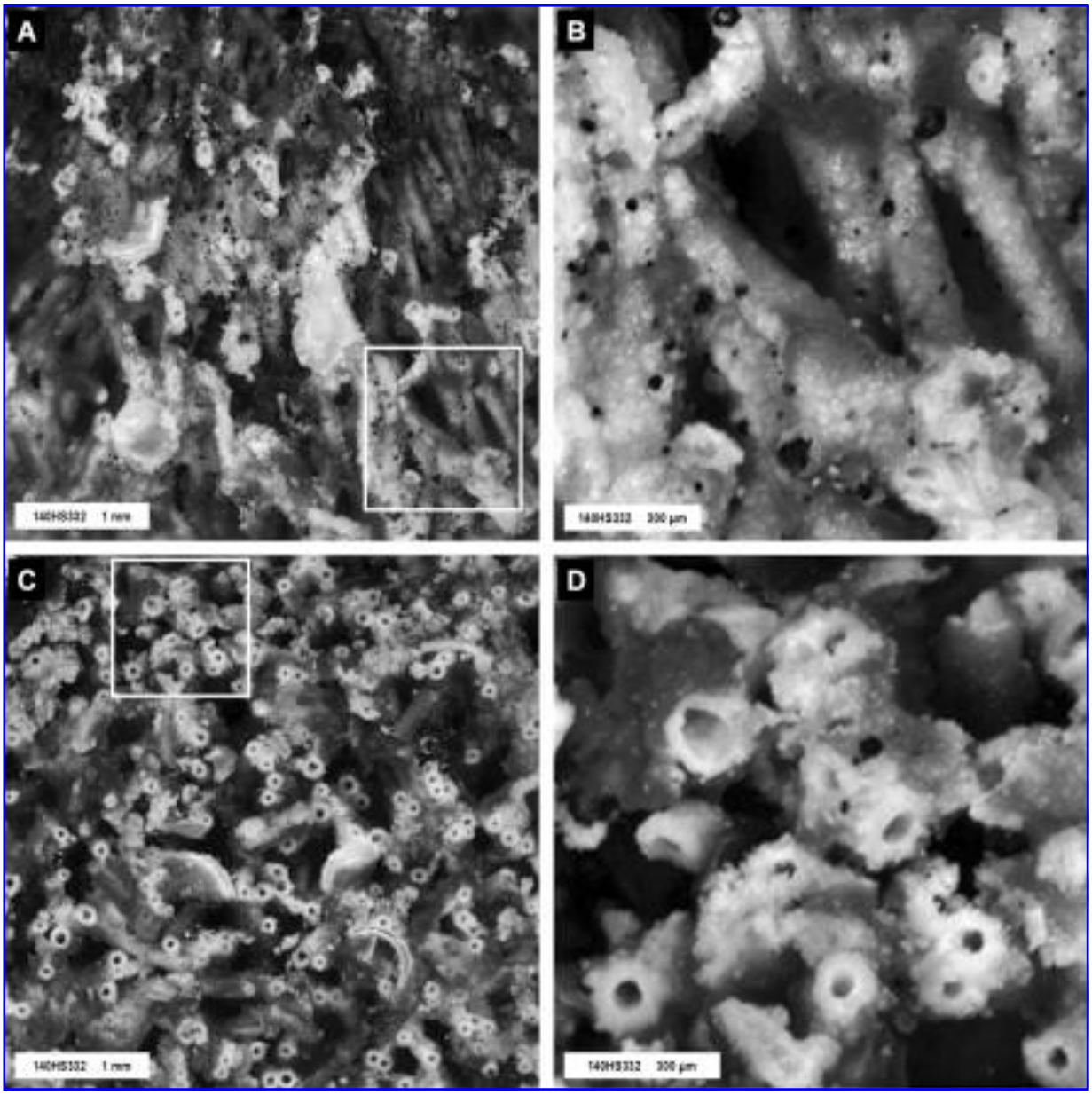

FIG. 9. ***In situ*** **microscopic imaging of sample 140HS332 (freshwater limestone, Ries Crater, Germany).** (**A**) Fresh surface showing tubular fabric in longitudinal section. (**B**) Close-up of individual tubes highlighted in full-frame view (A). Note the encrusted texture of the exterior of the tubes and isolated black spots (organic compound). The tubes were formed around threadlike cyanobacteria *Cladophorites* by calcification and later dolomitization. (**C**) Fresh surface showing tubes in cross section. Note the consistent morphology and hollow cores. (**D**) Close-up view of region highlighted in full frame view (C). Instrumentation: Beagle 2 QM microscope. Image credits: PAFSnet.

dolomitic matrix/veneer are consistent with the environment of deposition and what is known about calcifying microbial filaments in such environments. Although no carbon was observed directly within the filaments, spots of organic carbon that have the characteristics of degraded carbon of biogenic origin are widely dispersed over the filaments. This carbon could, of course, have an extraneous origin and may not necessarily be related to the potentially biogenic filaments. However, the morphological and mineralogical parameters of 140HS332 and related samples on their own suggest that there is a strong likelihood the tubes actually represent mineralized microbial filaments (and the smooth films are probably microbial biopolymer or extracellular polymeric

TABLE 3. XRD DATA (SUMMARIZED)

Sample	*Powder*[a]	*Field sample*[b]
140: Limestone	Dolomite and calcite Quartz (probably detrital)	Calcite with dolomite (fresh tubes) Dolomite with minor calcite (matrix/veneers) See Fig. 10
169: Opaline sinter	Amorphous silica (opal)	Not analyzed
45: Chalcedony	Quartz with hematite	Not analyzed
179: Goethite	Goethite	Not analyzed
114: Orthoquartzite	Quartz	Quartz with calcite (all surfaces) Amorphous substance (silica) (matrix)
194: Marble	Dolomite, calcite and kaolinite	Not analyzed
44: Selenite	Gypsum	Not analyzed

[a]Philips PW1710 diffractometer, Department of Geology, University of Leicester, Leicester.
[b]Microsource® and INEL PSD, Department of Mineralogy, Natural History Museum, London.

substances). We therefore conclude that, on the basis of the observations and biogeochemical analyses, the evidence for a biogenic origin for this specimen is strong. Sampling and further analysis would, therefore, be justified.

Opaline Sinter, Yellowstone Park, Wyoming, USA (169)

External surfaces of sample 169HS330 (parallel to the layering) are smooth, weathered, and dis-

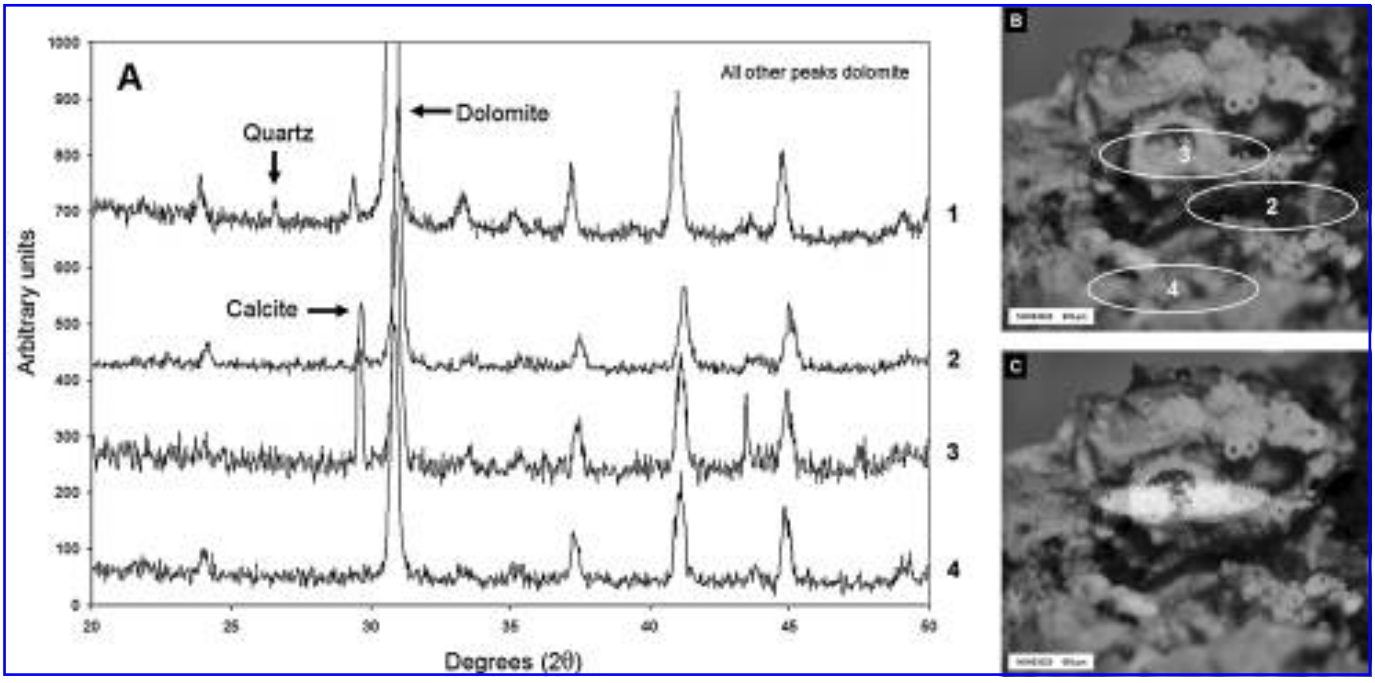

FIG. 10. ***In situ*** **XRD analysis of sample 140HS332 (freshwater limestone, Ries Crater, Germany).** (**A**) Comparison of spectra from prepared bulk powder (1) and three *in situ* targets on sample 140HS332 (2–4). Powder analyzed by standard lab diffractometer (range 0° to 65° 2θ, Cu-Kα radiation, Ni filter) and field specimen by an *in situ* diffractometer (range 0° to 120° 2θ, Cu-Kα radiation, no filter). Calcite is associated with the "white" tubes, but dolomite pervades throughout. The occurrence of quartz in the powder sample may be due to detrital contamination. Slight lateral shift in the powder spectrum is due to uncorrected instrument alignment. (**B**) Location of *in situ* targets (ellipses) on sample 140HS332 (scale bar is 0.6 mm). (**C**) Beam footprint of the *in situ* instrument (target 3 example). *In situ* data and images courtesy of Department of Mineralogy, Natural History Museum, London. Powder data courtesy of Department of Geology, University of Leicester.

TABLE 4. *IN SITU* RAMAN SPECTROSCOPY DATA (SUMMARIZED)

Sample	*Mineralogy and organics*
140: Limestone	Calcite [fresh tubes (white masses)]; Dolomite (general matrix, outer zones of fresh tubes, within tube interiors); Gypsum (isolated spots within general fabric); Unknown organic compound (broad band) (isolated black spots in matrix)
169: Opaline sinter	Not analyzed
45: Chalcedony	Not analyzed
179: Goethite	Not analyzed
114: Orthoquartzite	Quartz with minor gypsum (fresh and case-hardened exterior); Hematite (red band and case-hardened exterior); Scytonemin and chlorophyll (black and white zones); Ca-oxalate monohydrate (whewellite) (black and white zones); Quartz with rutile (white zone below red band). Note: Hematite is more concentrated in red band compared to exterior.
194: Marble	Dolomite (all surfaces); Quartz, goethite, olivine (detrital?) (pink zone); Scytonemin, carotene (astaxanthine?) (black zone); Carotene (echinenone?), chlorophyll (pink zone); Scytonemin (green zone); Carotene (possibly zeaxanthin and probably β-carotene) (blue zone); Something akin to c-phycocyanin[a] (blue zone)
44: Selenite	Gypsum (all surfaces); Carotene, scytonemin and chlorophyll (colony A) Carotene, parietin and chlorophyll (colony B). Note: Colony A has less carotene and more chlorophyll than colony B.

Bruker IFS66 IR spectrometer with FRA 106 Raman module and Nd3+/YAG laser (1064 nm) in conjunction with a Raman non-confocal microscope and Renishaw *InVia* confocal Raman microscope (488 nm, 514 nm, and 785 nm). Department of Chemical and Forensic Sciences, University of Bradford, UK.

[a]Blue accessory pigment is associated with photosynthetic membranes and accounts for up to 20% of protein in cyanobacteria.

colored. Macroscopic camera images document a very heterogeneous structure that consists of parallel laminae and layers that have a predominantly vertical fibrous fabric (Fig. 1b). Oval-to-round void spaces are common. Stereo macroscopy (Fig. 13) showed the fibrous structure more clearly, with the alternating fine parallel laminae interspaced by vertical columns between which void spaces occur. Individual fibrous threads, some tens to about 100 μm in diameter, stretch across the void space of the cavities in a webbed fashion. Microscopic observation of the weathered external surface as well as an unweathered fresh surface showed details of the threads that form a thickly, but finely intertwined, matted or webbed network. The threads at this scale are of the order of 8–20 μm in diameter.

XRD confirmed the dominant mineral to be amorphous silica (Table 3). Low bulk iron content was reported by Mössbauer spectroscopy (Table 5) with the external surfaces exhibiting a slightly higher abundance than fresh surfaces.

Biogenic evaluation

As with the Ries Crater samples (*i.e.*, 140HS332), the macroscopically visible heterogeneous structure of 169HS330, which consists of fibrous parallel laminae interspaced with vertical columns with visible webbed threads that span void spaces, is immediately suggestive of a biological structure related to microbial mat–forming behavior. The matted, webbed threads that form the construct reinforce this impression. The siliceous composition is consistent with that of a microbialite formed in a siliceous hot-spring environment. Indeed, the threads may represent bundles of several individual silica-encrusted filaments that range from 8–20 μm in diameter [compare Fig. 7 in Cady and Farmer (1996)]. It should also be noted that Cady and Farmer (1996) observed that the organic component of such opaline microbial sinters from Yellowstone hot springs had been removed through oxidation. On the basis of the morphological and compositional information, it is possible to conclude that the probability of biogenicity is high. Sampling and further analysis would, therefore, be justified.

Chalcedony, Cady Mountains, California, USA (45)

45HS265 is a sample of subsurface vein chalcedony, characterized by a heterogeneous external and internal texture that in some places appears to be fibrous (Figs. 1c and 14a). Microscopic

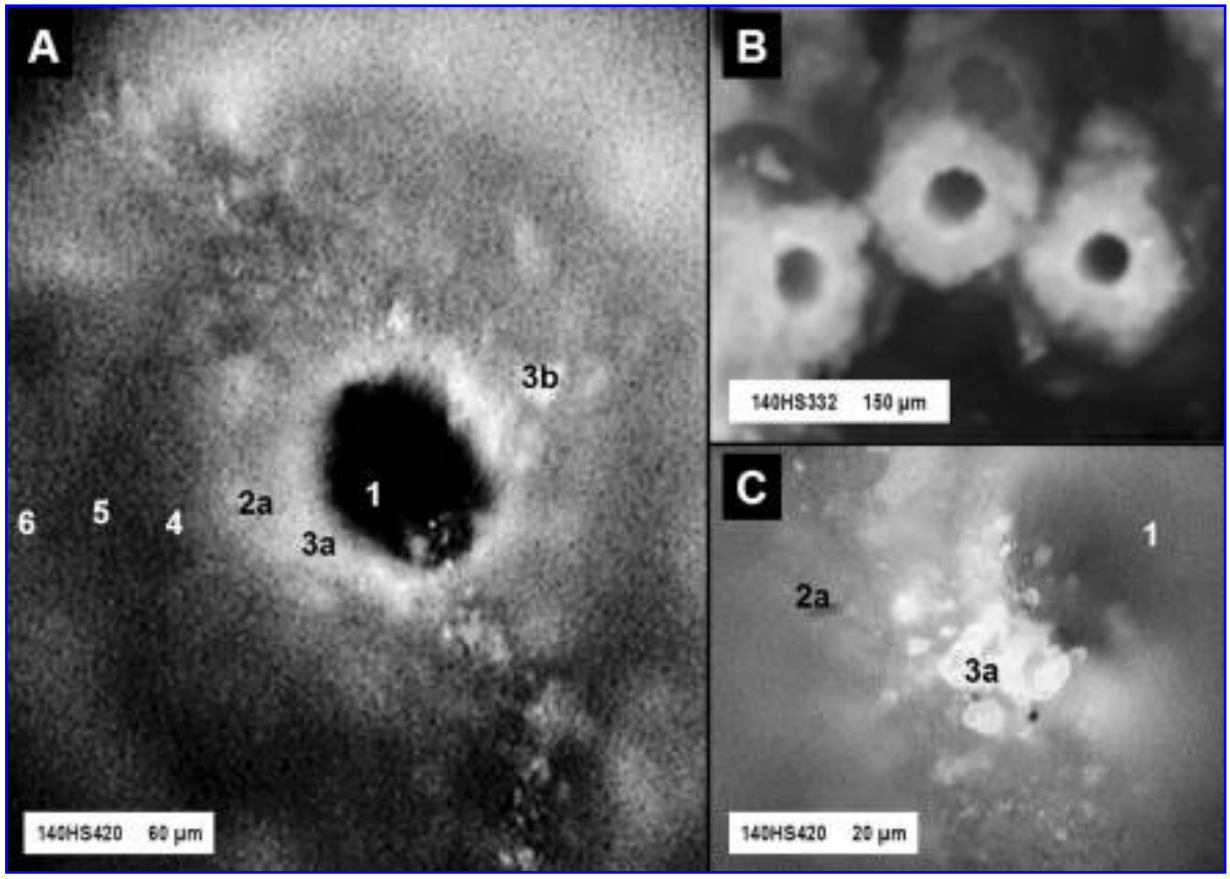

FIG. 11. Micro-Raman analysis of sample 140HS420 (freshwater limestone, Ries Crater, Germany). See Table 4. (**A**) Location of laser targets across the face of a single tube from outer edge (6) to inner wall (1). (**B**) Context image showing calcified tubes in cross section (sample 140HS332). (**C**) Close-up view of (A) showing area of calcite with minor dolomite (1), calcite and dolomite mix (2a) and isolated gypsum (3a). Instrumentation: Renishaw *InVia* confocal microscope operating at 785 nm and 514 nm (left and bottom right) and Beagle 2 QM microscope (top right). Image credits: PAFSnet.

details of the fibrous areas show that they are formed of parallel layers of mineral-encrusted tubes that range from ~20 μm to ~300 μm in diameter (Fig. 14b). Isolated thread-like features (~10 μm thick) occur within void spaces.

Sample 45HS265 is predominantly red, but the external surfaces are noticeably more yellow, which suggests that 2 iron phases are present. High reflectance on the surface of this sample is due to the presence of quartz. Mössbauer data confirm the presence of hematite and goethite, with the latter more abundant on external surfaces (Table 5 and Fig. 15), thus tallying with the observed coloration. XRD confirmed the presence of hematite and quartz by bulk analysis (Table 3), probably due to the derived powder being sourced from internal material only. Interestingly, the XRF showed concentrations of heavy metals, such as As, Pb, Cu, and Zn, possibly related to hydrothermal fluids.

Biogenic evaluation

The heterogeneous fibrous texture of 45HS265, plus matted, hollow tubes, are suggestive of a microbial origin, but more (targeted) microscopic details of the matted fabric and mineral-encrusted filaments, as well as Raman indication of the presence of organic matter (if any), would be useful for biogenic interpretation. The compositional data are suggestive of formation of a deposit in a hydrothermal environment, thus a habitable zone. We conclude that the evidence for biogenicity is moderately strong; more detailed morphological observations and organic carbon analyses would be useful. Sampling may be jus-

TABLE 5. *IN SITU* MÖSSBAUER SPECTROSCOPY DATA (SUMMARIZED)

Sample	*Fe-mineralogy*
140: Limestone	Octahedral Fe^{3+} (tubes) Octahedral Fe^{3+} (external sintered surface) Note: Effect more pronounced on fresh surfaces where tubes are presented in cross section
169: Opaline sinter	Octahedral Fe^{3+} (fresh surface) Octahedral Fe^{3+} (external surface) Note: Low signal (all surfaces). Slightly increased effect on external surfaces compared to fresh surfaces
45: Chalcedony	Crystalline goethite and hematite (external surface) Hematite and crystalline goethite (internal surface) Note: External goethite probably linked to yellow coloration (more pronounced on external surface) and hematite to red coloration (more pronounced on internal surface)
179: Goethite	Octahedral Fe^{3+} attributed to goethite (all surfaces)
114: Orthoquartzite	Red coloration of exterior and Fe-mobilized zone attributed to small amounts of octahedral Fe^{3+} (probably as thin grain coatings) Note: Low signal (all surfaces)
194: Marble	Not analyzed
44: Selenite	Not analyzed

Beagle 2 QM Mössbauer spectrometer, University of Mainz, Germany.

tified on these grounds, but the decision would depend on the payload.

Goethite, Cerro de Pasco, Peru (179)

The finely laminated, fibrous surface texture of sample 179HS367 is evident in proximal images (Figs. 1d and 16a). Macroscopic stereo imaging confirmed an open, framework texture, and microscopy showed further details of the filaments in plan and cross section (Fig. 16b). Although there is an overall parallel fabric, intertwining of the filaments is also apparent. Threads of various sizes (60–200 μm diameter) can be discerned, and unlike sample 140HS332 (Ries limestone) they are not hollow. Botryoids festoon the surface, and some follow the filaments along their length. Others exhibit what appear to be regular septate di-

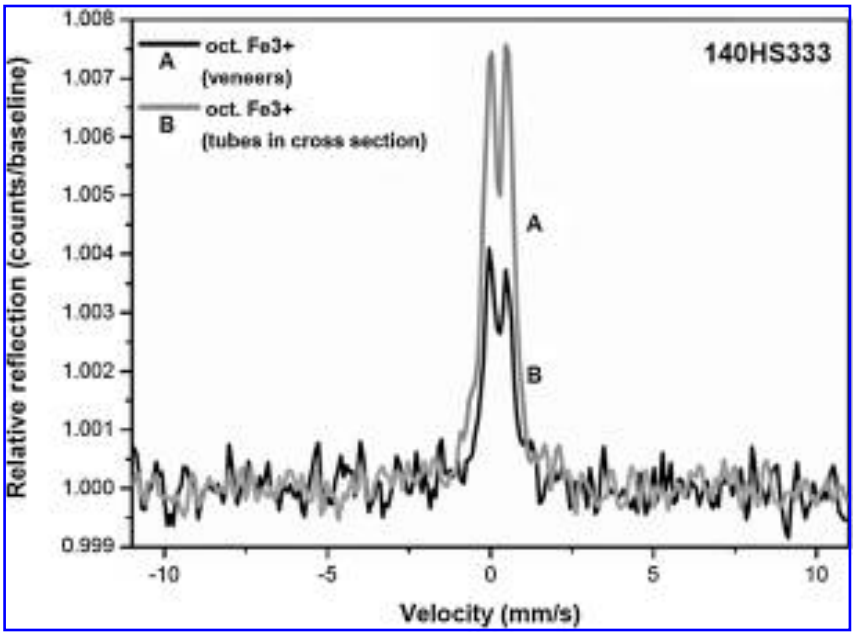

FIG. 12. ***In situ*** **Mössbauer spectra of sample 140HS333 (freshwater limestone, Ries Crater, Germany) showing difference in iron content between dolomite veneers (A) and exposed tube surfaces (B).** Instrumentation: Beagle 2 QM Mössbauer Spectrometer. Data courtesy University of Mainz, Germany.

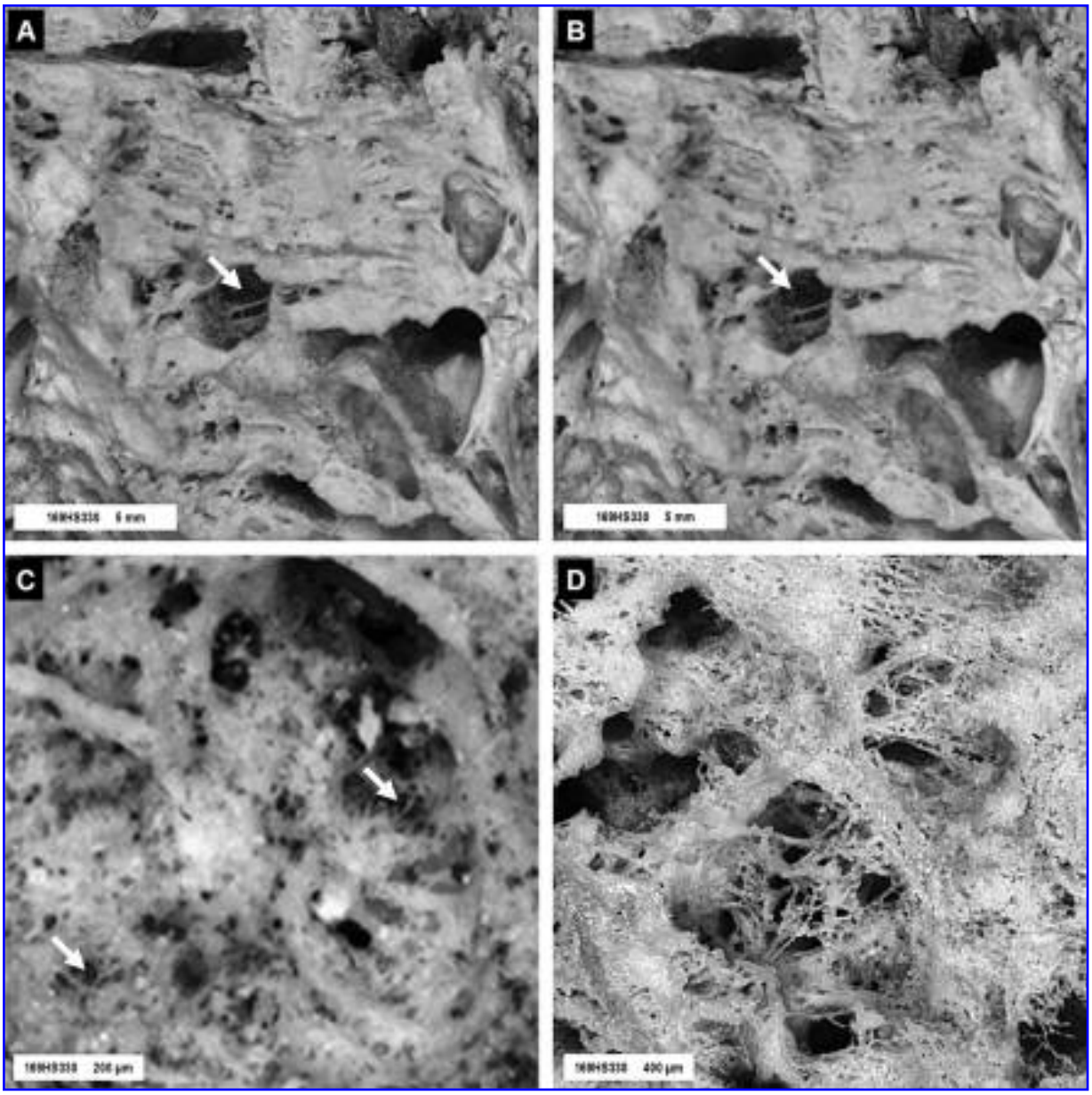

FIG. 13. ***In situ*** **macroscopic and microscopic imaging of sample 169HS330 (opaline sinter, Yellowstone Park, USA).** (**A** and **B**) Stereo pair acquired with single camera at 80 mm using ×6.4 close-up lens filter. Fresh surface with evident layered fabric and numerous voids, some containing threadlike features. (**C**) Isolated filaments preserved on external weathered surface. (**D**) Fresh surface showing well-preserved encrusted filaments within voids. Instrumentation: Beagle 2 DM stereo camera (A and B) and QM microscope (C and D). Image credits: PAFSnet.

visions (Fig. 16b). Smaller filaments of about 50–60 μm in diameter are characterized by platy septal divisions of the order of about 25 μm, whereas larger filaments, about 100 μm in diameter, consist of regular chains of 100 μm spheres.

Color imaging revealed the lustrous nature of the surface related to its metallic composition (equivalent to Fig. 16b). XRF data reveal high iron content (~34 wt% oxide), and goethite composition was confirmed by both XRD (Table 3) and Mössbauer spectroscopy (Table 5). Arsenic values are consistent with concentrations reported from this locality (Hofmann, personal communication). Expected high levels of trace Pb and Zn were not recorded *in situ* by XRF (Table 2), and the questionably high Mo values are attributed to instrumentation error (Phil Potts, Open University, personal communication).

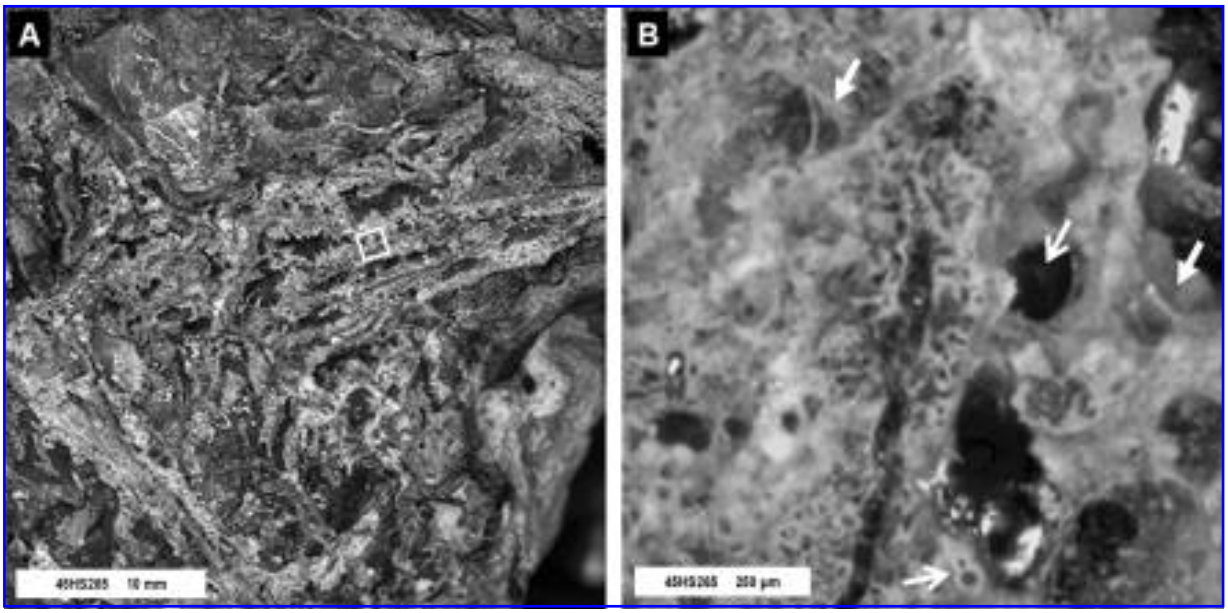

FIG. 14. ***In situ*** **macroscopic and microscopic imaging of sample 45HS265 (Fe-encrusted filaments in chalcedony vein, Cady Mountains, USA).** (**A**) Composite image acquired at 80 mm using the ×6.4 close-up lens filter and external RGB illumination (color not reproduced here). (**B**) Microscopic view of region highlighted in (A). Note the preserved filament strands (block arrows) and tubular voids in cross section (skeletal arrows). Instrumentation: Beagle 2 DM stereo camera (A) and Beagle 2 QM microscope (B). Image credits: PAFSnet.

Biogenic evaluation

As with the previously described samples, the interweaving, filamentous texture of 179HS367 is suggestive of biological behavior. The presence of regular septate divisions along the lengths of some of the filaments (Fig. 16b) is also characteristic. The fact that there are 2 types of division, depending on filament diameter, is an additional diagnostic aid for identification. The likelihood that these filaments represent iron oxide mineralized microbial filaments is, therefore, relatively high. This specimen would be a strong contender for sampling and further analysis.

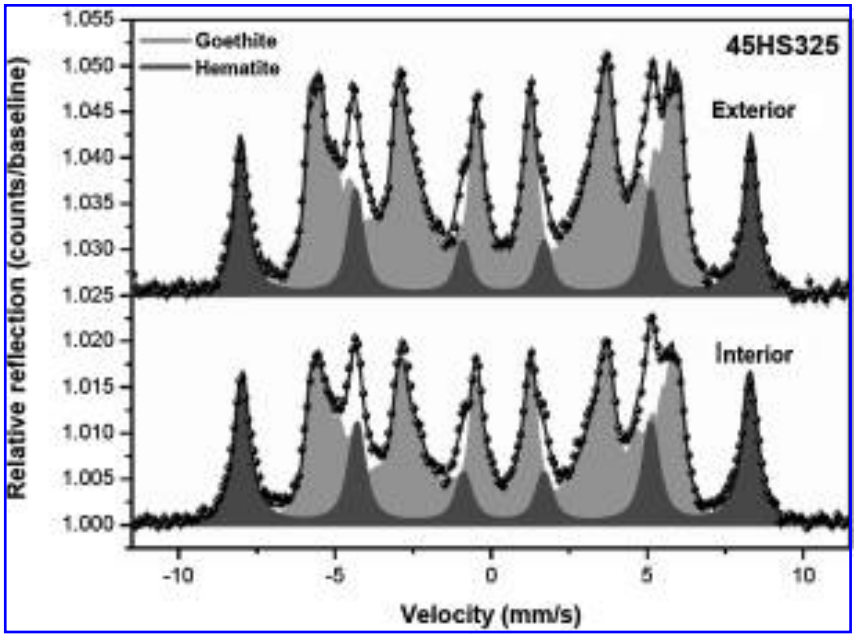

FIG. 15. ***In situ*** **Mössbauer spectra of sample 45HS325 (Fe-encrusted filaments in chalcedony vein, Cady Mountains, USA).** Two iron phases are present, hematite and goethite. Goethite is more pronounced on external (more yellow) surfaces. Instrumentation: Beagle 2 QM Mössbauer Spectrometer. Data courtesy University of Mainz, Germany.

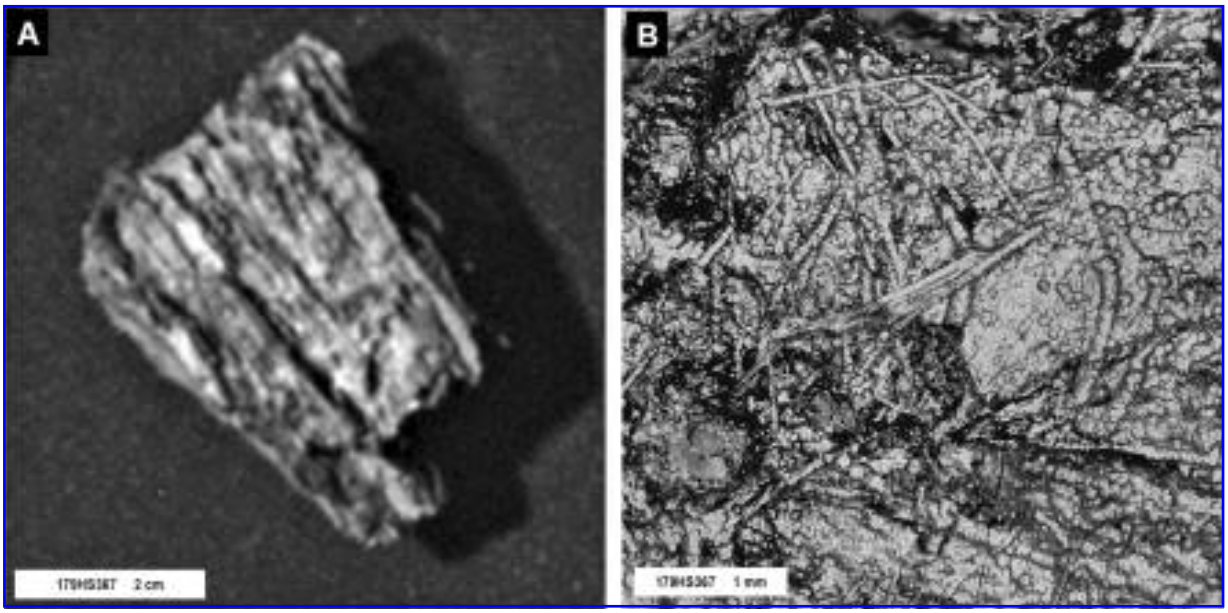

FIG. 16. Multi-scale imaging of sample 179HS367 (goethite, Cerro de Pasco, Peru). (**A**) Proximal image acquired at 60 cm using 750 nm filter (color-composite imaging at this range confirms a metallic luster). Macroscopic stereo imaging at 80 mm using the same camera (not shown) confirms a highly open fabric with well-preserved filament-like features draping the surface (see Fig. 1d). (**B**) Microscopic imaging displays a linear/chaotic filamentous fabric. Originally chemosynthetic hydrothermal microbes acted as substrates for the development of oxidation minerals, resulting in well-preserved signatures. Instrumentation: Beagle 2 DM stereo camera (A) and QM microscope (B). Image credits: PAFSnet.

Endoliths

Endoliths are generally 2-dimensional targets at the macroscopic and microscopic scale. Samples that contain cryptoendoliths required splitting to expose a vertical sequence or lateral exposure to the lichen layer at the exfoliating interface (*i.e.*, 114HS353). Chasmoliths, on the other hand, were exposed on surfaces, following splitting along host fractures (*i.e.*, 194HS435), or remained sandwiched between laminae when imaging could be performed through the host medium (*i.e.*, 44HS419). Multi-spectral imaging at all 3 scales was particularly successful for one of the specimens (194HS435). Ultraviolet imaging of this sample also revealed some organic compounds, which were identified by Raman spectroscopy to have detectable biofluorescent properties while others did not.

Orthoquartzite, McMurdo, Victoria Land, Antarctica (114)

Visually, samples 114HS353A and 114HS353B have a fine-grained homogeneous texture with areas of coloration, which is especially evident on the pronounced exfoliation planes (Fig. 17a) where mingled black and green-blue mottling can be seen. The external surface is distinctly orange-brown in color, which suggests an iron-coated surface that provides a striking contrast with the almost white, fresh interior. A fresh vertical section reveals distinct layering that consists of an almost colorless outer crust beneath which is a black zone that parallels the outer surface (Fig. 17c). The top contact of the black zone is sharp, whereas the lower contact diffuses into the rock. A whitish layer below the black zone is bordered below by a parallel, diffuse reddish brown zone.

Under UV illumination, areas of the sample within the white zone exhibited fluorescence (Fig. 18b) clearly associated with intergranular dark spots and other regions observed in the visible images (Fig. 18a). The black zone itself did not show any signs of fluorescence (Fig. 18b).

Quartz is the dominant mineral, as is evident from the XRD and Raman data (Tables 3 and 4, respectively). Multi-spectral imaging emphasized the layering pattern parallel to the outer surface of the rock and confirmed a spectral correspondence between the Fe-mobilization zone and the external surface (Fig. 17d). The finely reticulate texture of the iron-rich component seen in the spectral image indicates that the iron is

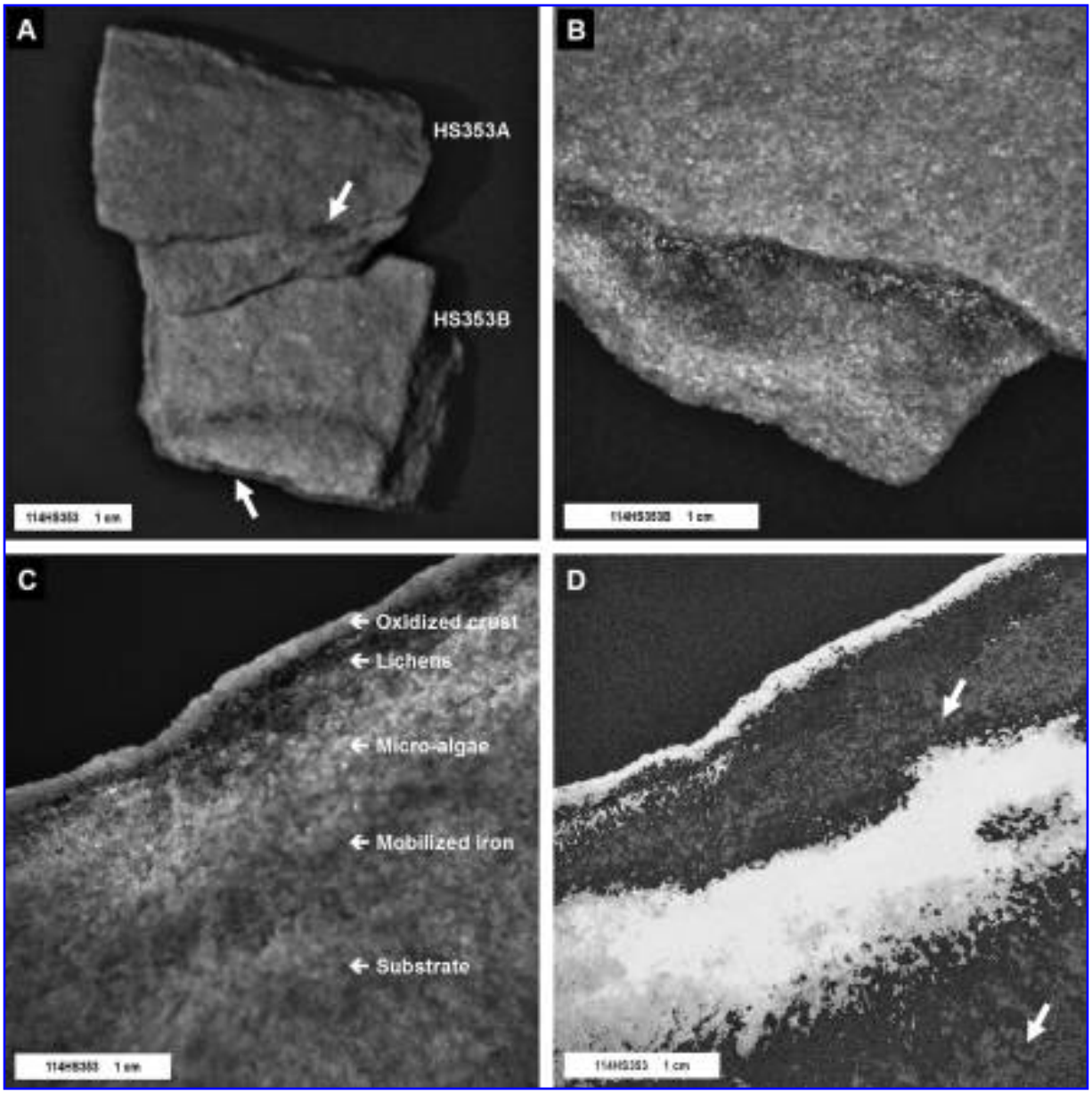

FIG. 17. ***In situ*** **proximal and macroscopic imaging of sample 114HS353 (orthoquartzite, McMurdo Dry Valleys, Antarctica).** (**A**) Proximal image acquired at 60 cm using 670 nm, 530 nm and 800 nm filters (color not reproduced here). The 800 nm filter was used in lieu of the blue filter (440 nm) (see text). The case-hardened exterior (HS353A) and iron mobilization zone (HS353B) are distinctly red in color images. The lichen zone is also discernable (arrows) on exfoliated surfaces (HS353A) and in cross section (HS353B). (**B**) Composite image acquired at 80 mm using ×6.4 close-up lens filter and external RGB illumination (see text). Cryptoendoliths exposed following exfoliation. Note the extent of the lichens (black). (**C**) Context image of specimen in cross section showing the zones described in Fig. 2. (**D**) Spectral image of the equivalent FOV as viewed between 420 nm and 720 nm. Regions containing iron are classified in white and quartz in black. Note the lichen layer is opaque within this range. Interstitial iron (as grain coatings) is inferred from the mottling within the fresh regions (arrows). Instrumentation: Beagle 2 DM stereo camera (A and B) and Nuance system (C and D). Image credits: PAFSnet.

probably present as a coating on individual grains. XRF confirmed the presence of a modest amount of iron (0.25 wt%, Table 2), but the low Mössbauer signal (Table 5 and Fig. 19) and no indication from XRD suggests that what is present is probably a very thin granular coating. Raman, however, identified the iron oxide as hematite (Table 4). The Raman data also indicates that a number of organic compounds, such as scytonemin, chlorophyll, and Ca-oxalate monohydrate are present in the black zone and the white, leached layer immediately below it (Table 4).

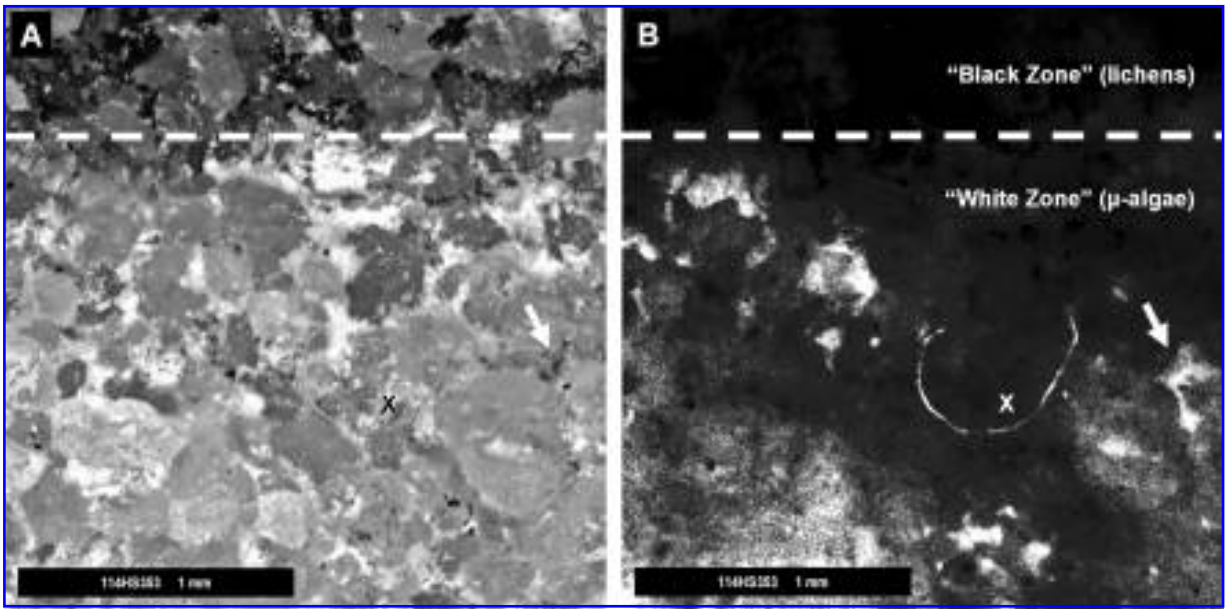

FIG. 18. ***In situ*** **microscopic imaging of sample 114HS353 (orthoquartzite, McMurdo Dry Valleys, Antarctica).** (**A**) Composite image acquired with the Beagle 2 microscope (color not reproduced here). Interstitial algae clearly visible within the "white zone" (black arrow). Iron coatings are not discernible. (**B**) Same FOV as in image (A) but using UV illumination only. Feature marked with an X is a synthetic fiber placed on the sample to assist in image processing. The lichen zone is uniformly opaque. Bright regions within the algal zone correspond to visible growth (as seen in A), but fluorescence also occurs elsewhere. Instrumentation: Beagle 2 QM microscope. Image credits: PAFSnet.

Biogenic evaluation

The Raman signatures are indisputably the main indicators of biogenicity within 114HS353. Other data, however, provide critical information for evaluating the life habitat. The light-colored, granular, slightly porous nature of this material indicates that it could be a suitable habitat for endolithic life-forms. Furthermore, the combination of distinct coloring on the exfoliated surfaces, the distinct layers of different colors parallel to the outer surface, and the presence of biofluorescence (not mineral fluorescence) associated with specific colored spots is additional evidence for the presence of extant endolithic microorganisms. Multi-spectral imaging confirmed that mobilization of iron occurred and re-precipitation was in a manner consistent with the behavior of endolithic microorganisms. Evidence for biogenicity in this sample is sufficiently strong to justify sampling and further analysis.

Marble, McMurdo, Victoria Land, Antarctica (194)

Sample 194HS435 has a coarsely crystalline, granular texture with intergranular Fe-oxide staining on more weathered surfaces (Figs. 3a and 20c). The rock is traversed by fractures that display areas of bluish coloration (first seen at the proximal scale) that, at closer scales, are made up of clusters of globular spots.

Dolomite mineralogy was confirmed by XRD (Table 3) and Raman spectroscopy (Table 4). *In situ* XRF could only confirm Ca content (~15 wt% oxide), since Mg cannot be recorded with the TN9000. Proximal imaging with the DM camera clearly identified blue-green areas on both fresh and internal weathered surfaces (Fig. 20a). Color macro-microscopy with the Beagle 2 cameras revealed these regions in more detail. The spectral signatures also indicate the presence of organic components associated with the colored areas on the fracture surfaces (Fig. 22).

Specimen 194HS435 provided an opportunity to detect biofluorescence in the form of globular spots at 2 scales with the Beagle 2 cameras (Fig. 21). Fluorescing areas of the sample were observed to coincide with the visible areas of coloration but also occurred in clear areas (compare Fig. 20d with highlighted region in Fig. 21b), which suggests that the distribution of the chasmoliths is more pervasive than can be visually determined. Some parts of the visible chasmolithic colonies did not fluoresce, which led us to assume that these may be associated with UV-protective pigments. Raman spectroscopy identi-

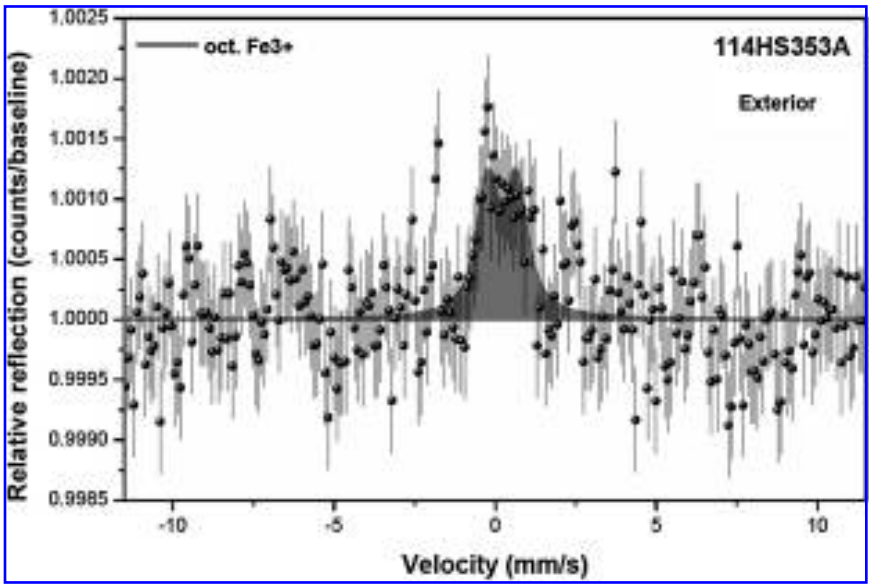

FIG. 19. ***In situ*** **Mössbauer spectrum of sample 114HS353A (orthoquartzite, McMurdo Dry Valleys, Antarctica).** The weak signal associated with external "oxidized" surfaces is due to iron being present as very thin grain coatings. Instrumentation: Beagle 2 QM Mössbauer Spectrometer. Data courtesy of University of Mainz, Germany.

fied various organic components across sample 194HS435 (Table 4). Chlorophyll and phycocyanin are likely candidates for the observed biofluorescence. Scytonemin (a radiation-protective pigment) occurs in both the blue-green regions and in black areas just under the external surface (Fig. 20b). A number of carotenes were also observed and tentatively identified (Table 4).

Biogenic evaluation

As with sample 114HS353 (orthoquartzite), the identification of a variety of biological organic components in 194HS435 by Raman spectroscopy constitutes an unambiguous compositional biosignature. Color and UV imaging allowed for the distribution of the biogenic organic components to be linked to the visible globular clusters on the fracture surfaces (morphological biosignature). Both imaging methods also showed that the chasmolithic organisms are more widely distributed than can be seen visually. The nature of the rock and the distribution of the organic biosignatures along fracture surfaces show that these organisms developed in a chasmolithic habitat. This rock would be a strong candidate for sampling and further analysis.

Gypsum, Haughton Crater, Devon Island, Canada (44)

Proximal and macroscopic imaging of 44HS419 revealed a pearly lustrous surface with a well-defined laminated structure (Fig. 23). In places, the sample is highly reflective (especially when imaged parallel to cleavage), but opaque spots and assemblages (chasmoliths) could still be readily observed macroscopically (Fig. 23c). Due to the clarity of the selenite, the distribution of interlaminar spots (chasmolithic microbial communities) could be determined vertically via the Beagle 2 microscope to ~20 μm by mapping in-focus regions within each image of the stack (Fig. 23d).

Calcium-rich composition was confirmed by XRF (Table 2) and gypsum mineralogy by XRD (Table 3) and Raman (Table 4). WDXRF analysis indicated low iron content (~0.05 wt% Fe_2O_3), and since no visual evidence of oxidized coatings was observed, Mössbauer spectroscopy was considered unnecessary. Raman spectroscopy revealed a variety of biogenic organic compounds, including carotene, scytonemin, chlorophyll, and parietin.

Biogenic evaluation

The correlation of biogenic compounds with the black spots seen within the cleavage planes of sample 44HS419 is clear evidence of their biogenicity. Their distribution between the cleavage planes of the colorless gypsum demonstrates the chasmolithic habitat. Targeted sampling and further analysis would be justified.

DISCUSSION

Unambiguous identification of generic biosignatures on Earth or Mars requires substantiating

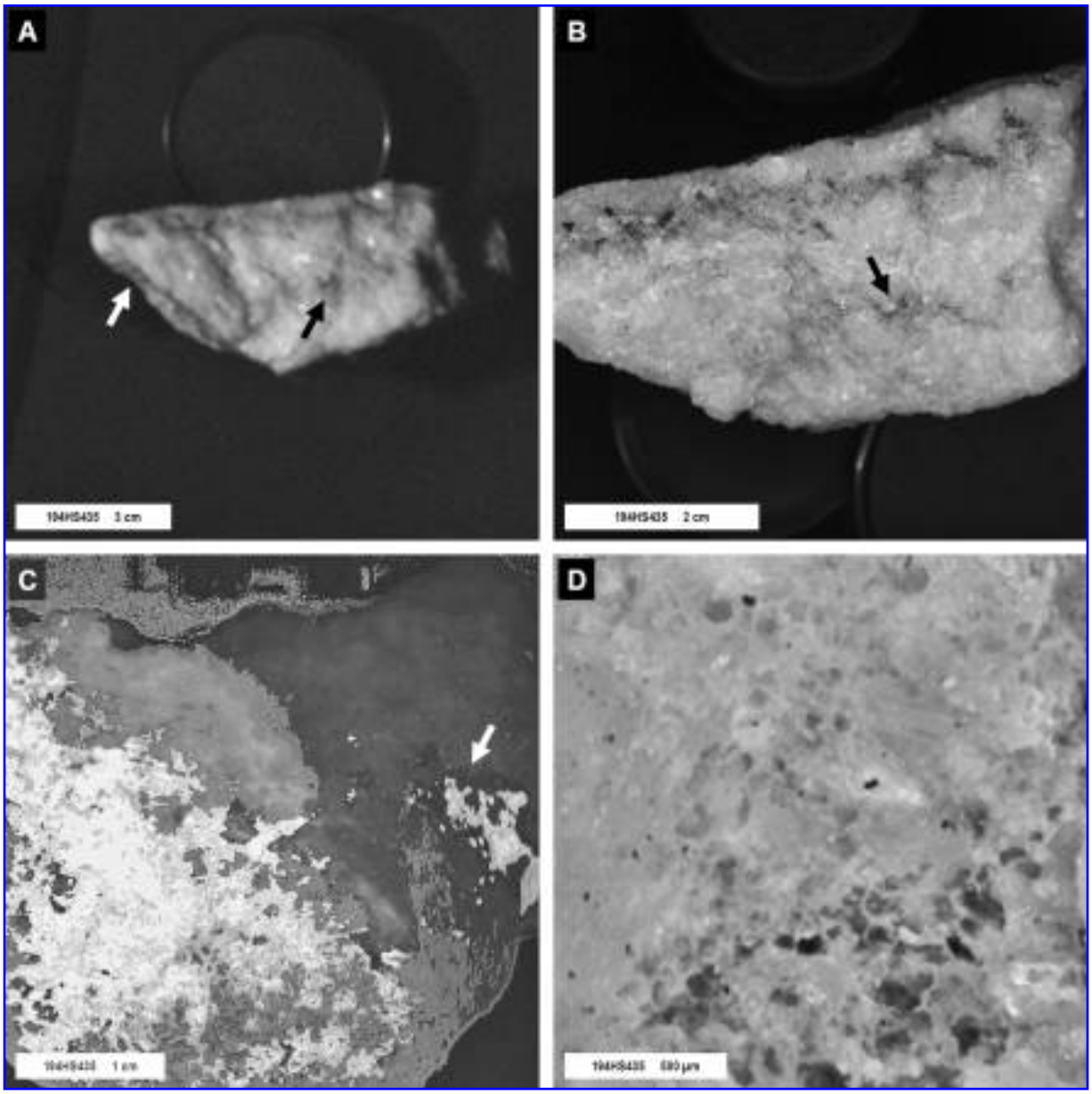

FIG. 20. Multi-scale imaging of sample 194HS435 (chasmolithic marble, McMurdo Dry Valleys, Antarctica). (**A**) Composite image acquired at 60 cm using 670 nm, 530 nm, and 800 nm filters (color not reproduced here). The 800 nm filter was used in lieu of the blue filter (440 nm) (see text). Arrows denote sites of cyanobacterial growth. (**B**) Composite image acquired at 80 mm using ×6.4 close-up lens filter and external RGB illumination (color not reproduced here; see text). Target identified in (A) clearly discernible as a blue band (arrow). This image has the same FOV as shown in Fig. 21a. (**C**) Spectrally classified macroscopic view of internal weathered surface (left of image) and fresh surface (right of image). Spectral range 420–720 nm. Fresh marble is classified in dark grey, chasmoliths in white, and weathered surface in light grey. Note the intergranular texture highlighted by the endolith signature (lower left of image). Exact FOV as shown in Fig. 3a. (**D**) Composite microscopic image of a region highlighted in (B). Colonies are arranged in globular masses and can be mapped visibly and by micro-Raman spectroscopy (see Table 4) and biofluorescence (see Fig. 21). Instrumentation: Beagle 2 DM stereo camera (A and B), Nuance camera system (C), and Beagle 2 QM microscope (D). Image credits: PAFSnet.

evidence from a multitude of techniques. It is scientifically poor to posit a biosignature based on evidence from one technique without corroboration from at least one other. This applies equally to morphological biosignatures observable within the scale range described in this study, which may have a detectable organic signature (114, 194, 44) or may be a residual biofabric formed as a re-

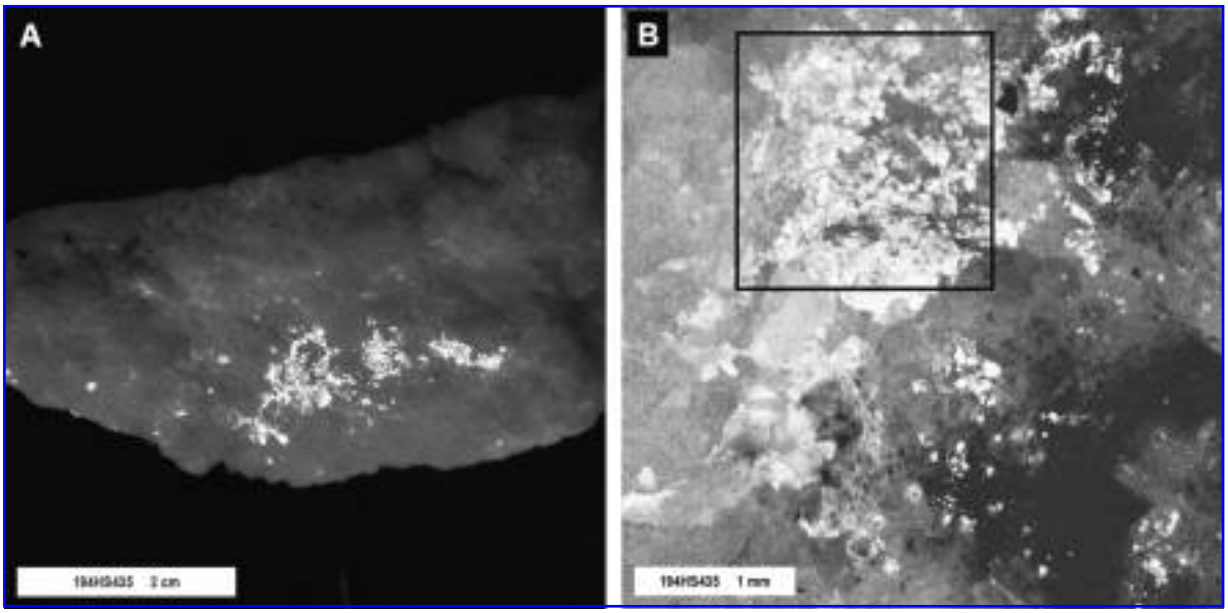

FIG. 21. ***In situ*** **macroscopic and microscopic UV fluorescence imaging of sample 194HS435 (chasmolithic marble, McMurdo Dry Valleys, Antarctica).** (**A**) Exact FOV as shown in Fig. 20b under external UV (365 nm) illumination only. Fluorescence coincides with blue areas and adjacent clear areas. (**B**) Detailed view of the microbial colonies using the Beagle 2 microscope and UV LEDs (373 nm) only. Comparisons with visible data (highlighted region is the same FOV as shown in Fig. 20d) indicates some areas are UV opaque, suggesting the presence of screening pigments such as scytonemin, later confirmed by Raman spectroscopy (see text). Instrumentation: Beagle 2 DM stereo camera (A) and Beagle 2 QM microscope (B). Image credits: PAFSnet.

sult of mineral encrustation (45, 140, 169, 179). The latter is a very common process observed on Earth and is entirely plausible for Mars (Banfield *et al.*, 2001). Corroborating evidence in support of morphological expression could come from a number of viable *in situ* observations, including physical properties, elemental chemistry, molecular chemistry, or mineralogy.

The structures observed in the majority of samples investigated in this study are relatively readily recognizable as biosignatures on the basis of morphology and composition. The rocks that contain extant endolithic microorganisms have an undeniably biogenic Raman biosignature, though the color and spectral imaging, as well as mineralogical composition, were necessary to provide information about the habitat and nature of the host rock. In the case of the mineralized microbial filaments, Raman spectroscopy was applied only to the freshwater limestone from the Ries impact crater (140); and the presence of spots of organic matter interspersed with the matted, mineralized filaments was a useful indicator, though not a conclusive one because of the possibility that the organic matter could have come from an extraneous source.

The work carried out in this study was by no means exhaustive, given the variety of potential planetary analogues available and the array of potential techniques possible. We did, however, investigate a number of fundamental sample attributes and methods applicable to *in situ* measurement within the constraints of current space instrument technology and established an approach upon which to build further.

From our archive of planetary analogue specimens, we selected a modest number of samples with which to investigate 2 morphological criteria that pertain to biology: mineralized microbial filaments and endolithic microorganisms (Table 1). As a collection, these samples are associated with relevant geological provenances (*i.e.*, impact sites, extreme habitats) and exhibit natural criteria, such as state of preservation and presentation (*i.e.*, fresh to weathered), morphology at the appropriate scale, chemomineralogical variation, and, in some cases, biofluorescence.

By definition, imaging is the most fundamental technique for identifying potential morphological biosignatures. To limit ambiguity in interpretation, as stated previously, it is crucial to complement visual evidence with analytical data.

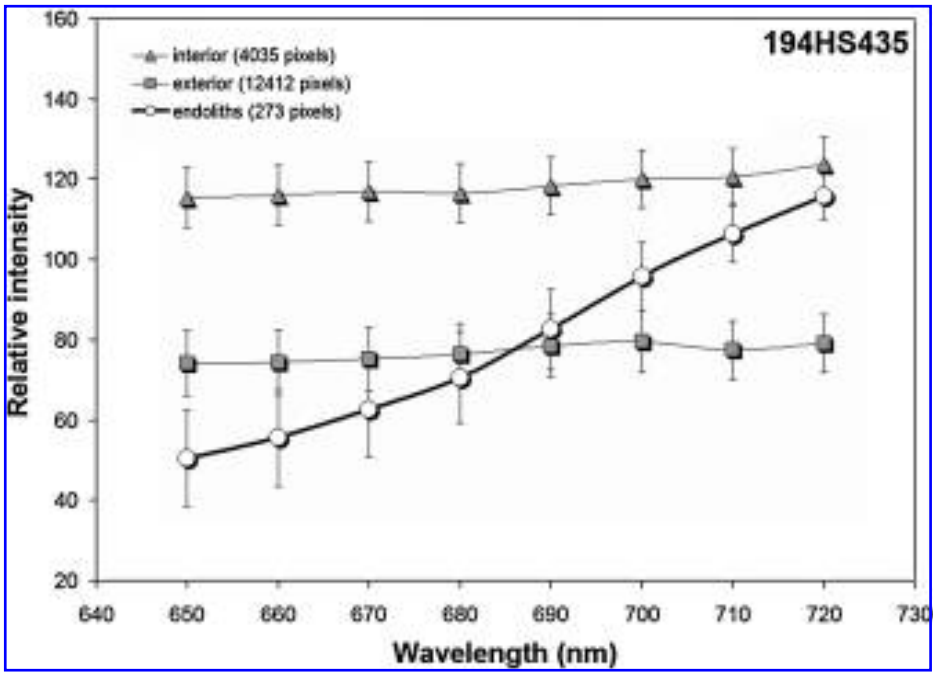

FIG. 22. ***In situ*** **multi-spectral macroscopic imaging of sample 194HS435 (chasmolithic marble, McMurdo Dry Valleys, Antarctica).** Spectral plots of selected regions of interest on the specimen observed between 650 nm and 720 nm. Size of each region indicated in pixels. The host mineralogy (dolomite) displays a flat response in this region of the visible spectrum, the only distinction being between the higher albedo (white) interior and discolored (brown) exterior. The steep positive gradient associated with regions displaying endoliths is characteristic of chlorophyll or similar organic compounds. Instrumentation: Nuance camera system courtesy of Newport LOT-Oriel. Image credit: PAFSnet.

For this study, we employed 4 techniques—XRF, XRD, Raman, and Mössbauer spectroscopy (Tables 2 through 5). With the exception of XRD, all are pre-sampling activities. For those rocks that contain extant life, Raman spectroscopy is fundamental. Access to potential targets is also crucial, and rock splitting is an obvious strategy to expose features without destroying them in the process (Fig. 6).

CONCLUSIONS

Collectively, all imaging, analytical, and geotechnical techniques that were employed confirmed their effectiveness for *in situ* astrobiology. The importance of a multidisciplinary approach was well demonstrated. By adopting a common sample philosophy (as would be the case during mission operations) and utilizing a combination of spaceflight hardware (where appropriate) and commercial instrumentation (acting as emulators), synergies, interdependences, and practical issues could be experienced firsthand. Scientifically, this study has also advanced our level of understanding of which techniques (available for this investigation and technologically viable for space missions) can be used in concert to evaluate the biogenicity of certain morphological features.

Based on the results of this initial study, some strategic criteria can be formulated (Table 6). A more detailed philosophy will emerge following the outcome of *in situ* studies within our broader program (*i.e.*, field experiments, sample preparation, robotics).

We introduce a practical scaling philosophy that defines radial working distances for *in situ* operational activities of stationed rovers, static landers, and "instrumented" humans: proximal (~100 cm), macroscopic (~10 cm) and microscopic (~1 cm). Our adoption of the term *proximal* allows us to correspond with the lower bounds of the microfacies scale (meters to centimeters) advocated by Cady *et al.* (2003). Strategies differ at each scale, and each is dependent upon the other. As such, spatial imaging should be seamless within this range of distances and have high spectral capability (bandwidth and resolution) to support each scale. Self-illumination

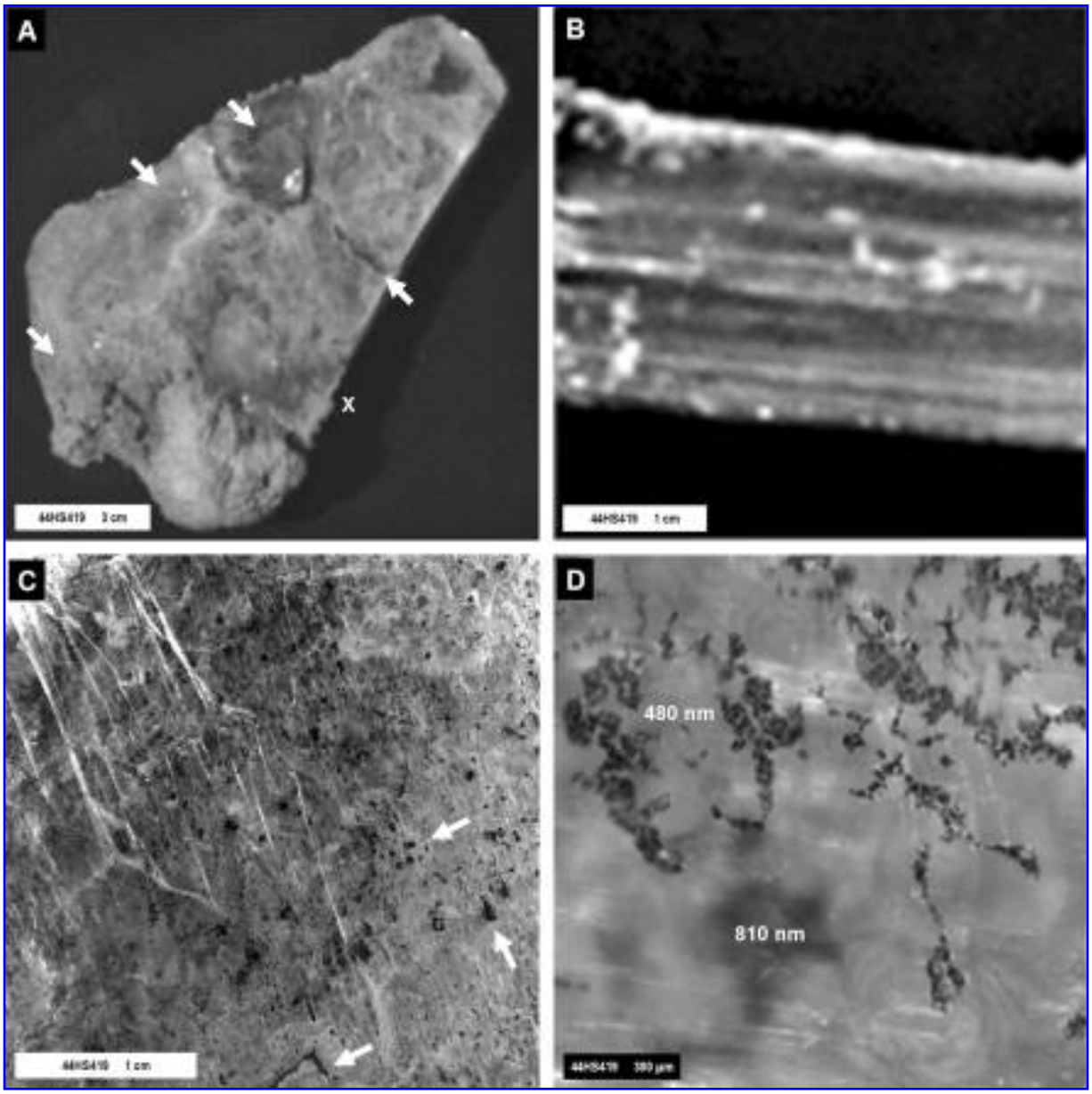

FIG. 23. ***In situ*** **imaging at all scales of sample 44HS419 (gypsum** ***var.*** **selenite, Haughton Crater, Devon Island, Canada).** (**A**) Proximal image acquired at 60 cm with a 670 nm filter. View is 90° to cleavage plane. Evidence for laminated fabric (areas marked with arrows). (**B**) Proximal image (670 nm filter) of sample in cross section (along edge marked X in top left). Laminations are clearly visible. Stereo macroscopy of this surface (not shown) reveals variable relief associated with very thin cleavage folia. (**C**) Macroscopic view (80 mm distance) of reverse side of specimen to that shown top left. Chasmoliths (black spots in image) are well distributed both spatially and vertically into the specimen (observable due to the transparency and clarity of the gypsum). (**D**) Microscopic view of chasmoliths. Note the globular/chainlike morphology of the colonies. Two vertically spaced colonies are shown, one in focus (480 nm below surface) and one out of focus (810 nm below surface). Instrumentation: Beagle 2 DM stereo camera (A and B) and QM microscope (C and D). Image credits: PAFSnet.

is useful for *in situ* macroscopy and essential for *in situ* microscopy, which provides a controlled way of obtaining the true color of targets and a means for identifying and discriminating bio-fluorescent features (via UV excitation).

The Nuance multi-spectral system, an example of a future technology for space, was extremely useful for macroscopic imaging (Figs. 8, 17, and 20) and should be exploited across the scale range. Microscopic imaging of some study sam-

TABLE 6. SUMMARY OF KEY FEATURES OBSERVED AT EACH WORKING SCALE DURING THIS STUDY

Working distance[a]	*Activity*	*Key features (sample family ID)*[c]
Proximal	Ambient (solar) illumination only	Spectral anomalies (194)
~100 cm	Stereo imaging (using standard methods such as pairs)	Evidence of layering (169, 114, 44)
	Multi-spectral classification of candidate targets	Sintered (140) and aligned textures (140, 179)
	Target selection for macroscopy (4 cm × 4 cm)	
Macroscopic	Ambient (solar) or self-illumination (RGB, UV)	Evidence of open fabric (140, 169, 179)
~10 cm	Stereo and 3-D imaging (using translation techniques)	Evidence of tubular morphology (140)
	Multi-spectral classification of observed features	Mineralogical association with morphology (140)
	True color imaging (RGB)	Visible filaments (45, 179)
	Check for UV fluorescence (biological or mineralogical)	Visible cryptoendoliths (114) and chasmoliths (44)
	Target selection for microscopy (4 mm × 4 mm)	Biofluorescence (194)
	Target selection for *in situ* XRF (spot diameter ~20 mm)	
	Target selection for *in situ* XRD (spot area ~0.13 mm^2)	
	Target selection for *in situ* Mössbauer (spot diameter ~14 mm)	
Microscopic[b]	Self-illumination (RGB, UV)	3-D morphology of tubes (140) and clusters (169)
~1 cm	Stereo and 3-D imaging (using translation techniques)	Morphology of Fe-encrusted filaments (45)
	True color imaging (RGB)	3-D distribution of chasmoliths (44)
	Check for UV fluorescence (biological or mineralogical)	Globular texture of chasmoliths (194, 44)
	Target selection for *in situ* Raman (spot size ~2 μm to 100 μm)	Distribution of biofluorescence (194)
	Geochemistry (XRF) and mineralogy (XRD, Raman, Mössbauer)	Trace element enrichment (140, 45)
	Organic compounds (Raman)	Fe-coated grains (114)
	Physical properties (geotechnics)	Identification of scytonemin (114, 194)
		Identification of carotenes (194, 44)
		Identification of chlorophyll (114, 194, 44)

[a]Distance between observer (instrument) and target (feature on sample).
[b]May involve physical contact to ensure correct standoff distance between detector and target.
[c]See text for explanation of sample IDs.

ples with the Beagle 2 microscope produced impressive results but often required additional care when fine positioning over a target identified at the macroscopic scale. This was particularly challenging when visible biosignatures were small and spatially disseminated (Fig. 14b). Three-dimensional imaging also proved invaluable for open fabric materials (Figs. 9, 13, and 14). Specular reflection was more of a problem for the DM camera than for the microscope due to a combination of non-diffused projected light from the commercial ring light and high reflectivity of some targets (Fig. 23c). Enhancements are already being implemented to minimize this effect. The Beagle 2 microscope performed exceptionally well and produced some spectacular results (Figs. 9, 13d, 16b, 21b, and 23d), which confirmed the usefulness of a true "deployable" field microscope. Incremental focusing could also be similarly beneficial for macroscopy. Stereo imaging may also benefit microscopy following the success with the DM camera (Fig. 13).

The analytical data generally confirm the composition of each host material, but *in situ* spot measurements (*i.e.*, XRD) provide more detail and help to discriminate variation in spatial composition (Fig. 10). Generally, the portable XRF, though limited in terms of elemental coverage, provided supportive evidence with which to assist in material classification (Table 2). Expanding the range, especially for major element analysis, will be a requirement for continued studies. Raman spectroscopy proved to be valuable as an *in situ* technique due to its ability to identify and map organic compounds (and mineralogy) precisely to the imaging data (Fig. 11). Mössbauer

spectroscopy, already a proven technique on Mars (Morris *et al.*, 2004; Klingelhöfer *et al.*, 2004; Morris *et al.*, 2006), was useful for certain samples (114HS353).

Future studies

Our work described here marks an initial step in acquiring practical experience with multiple *in situ* techniques for planetary exploration, which will inevitably be of benefit to planetary scientists, instrument designers, and mission engineers. Further work will be essential in order to build on this experience and maximize readiness for future missions to Mars.

With the expansion of our library of planetary analogue samples, many of which have astrobiological significance, we will be able to build a valuable database using the full array of techniques at our disposal. Some of the more interesting samples used in this study are single specimens, donated from other collections, and could not be analyzed by the range of techniques available to us. Future studies will require an adequate supply of samples, ideally those collected from the field specifically for the program.

The next steps will involve applications in the field (at analogous sites), sampling strategies (including rover operations and post-sampling laboratory experiments, *i.e.*, immunoassay) for more complete end-to-end simulations, blind tests, and additional *in situ* techniques we are yet to exploit. Geotechnics will also feature more in follow-up work. New techniques or instrument prototypes under development (*i.e.*, ExoMars hardware) will be included in our coordinated program as they become available.

ACKNOWLEDGMENTS

The authors gratefully acknowledge the following individuals and/or institutions for their valued contributions to this study: Phil Potts, Open University, UK (TN Spectrace 9000 portable XRF); Dean Talboys, University of Leicester, UK (Beagle 2 XRS); Nicholas Thomas and Benjamin Lüthi, University of Bern, Switzerland (Beagle 2 microscope); Andrew Coates and Andrew Griffiths, Mullard Space Science Laboratory, UK (Beagle 2 Stereo Camera System); Gernot Arp, University of Göttingen, Germany (Ries Crater studies); Tim Brewer and Kevin Sharkey, Department of Geology, University of Leicester, UK (WDXRF/XRD); and David Fletcher-Homes, CRI Inc., USA (Nuance system). Derek Pullan acknowledges PPARC for funding part of the work carried out at the University of Leicester under grant RP16082, and EPSRC, via TREATAE and the University of Aberdeen, for providing additional financial support to disseminate and promote this work.

ABBREVIATIONS

DM, Development Model; FOV, field of view; FS-XRS, Flight Spare X-ray spectrometer; PAFS-net, the Planetary Analogue Field Studies Network; PAW, Position Adjustable Workbench (on Beagle 2); PSD, position-sensitive detector; QM, Qualification Model; WDXRF, wavelength dispersive X-ray fluorescence; XRD, X-ray diffraction; XRF, X-ray fluorescence; XRS, X-ray spectrometer.

REFERENCES

Arp, G. (1995) Lacustrine bioherms, spring mounds, and marginal carbonates of the Ries-impact-crater (Miocene, southern Germany). *Facies* 33, 35–90.

Arvidson, R.E., Anderson, R.C., Bartlett, P., Bell, J.F., III, Blaney, D., Christensen, P.R., Chu, P., Crumpler, L., Davis, K., Ehlmann, B.L., Fergason, R., Golombek, M.P., Gorevan, S., Grant, J.A., Greeley, R., Guinness, E.A., Haldemann, A.F.C., Herkenhoff, K., Johnson, J., Landis, G., Li, R., Lindemann, R., McSween, H., Ming, D.W., Myrick, T., Richter, L., Seelos, F.P., IV, Squyres, S.W., Sullivan, R.J., Wang, A., and Wilson, J. (2004a) Localization and physical properties experiments conducted by Spirit at Gusev Crater. *Science* 305, 821–824.

Arvidson, R.E., Anderson, R.C., Bartlett, P., Bell, J.F., III, Christensen, P.R., Chu, P., Davis, K., Ehlmann, B.L., Golombek, M.P., Gorevan, S., Guinness, E.A., Haldemann, A.F.C., Herkenhoff, K., Landis, G., Li, R., Lindemann, R., McSween, H., Ming, D.W., Myrick, T., Parker, T., Richter, L., Seelos, F.P., IV, Soderblom, L.A., Squyres, S.W., Sullivan, R.J., and Wilson, J. (2004b) Localization and physical properties experiments conducted by Opportunity at Meridiani Planum. *Science* 306, 1730–1733.

Awramik, S.M. and Grey, K. (2005) Stromatolites: biogenicity, biosignatures, and bioconfusion. *Astrobiology and Planetary Missions: Proceedings of the SPIE*, Vol. 5906, edited by R.B. Hoover, G.V. Levin, A.Y. Rozanov, and G.R. Gladstone, SPIE—The International Society for Optical Engineering, Bellingham, Washington, pp. 227–235.

Baglioni, P. (2003) *Pasteur Payload Package: Instrument Definition Document*, European Space Agency, Paris.

Banfield, J.F., Moreau, J.W., Chan, C.S, Welch, S.A., and Little, B. (2001) Mineralogical biosignatures and the search for life on Mars. *Astrobiology* 1, 447–465.

Bishop, J.L., Murad, E., Lane, M.D., and Mancinelli, R.L. (2004) Multiple techniques for mineral identification on Mars: a study of hydrothermal rocks as potential analogues for astrobiology sites on Mars. *Icarus* 169, 311–323.

Blackhurst, R.L., Genge, M.J., Kearsley, A.T., and Grady, M.M. (2005) Cryptoendolithic alteration of Antarctic sandstones: pioneers or opportunists? *J. Geophys. Res.* 110, E12S24.

Boston, P.J., Spilde, M.N., Northup, D.E., Melim, L.A., Soroka, D.S., Kleina, L.G., Lavoie, K.H., Hose, L.D., Mallory, L.M., Dahm, C.N., Crossey, L.J., and Schelble, R.T. (2001) Cave biosignature suites: microbes, minerals and Mars. *Astrobiology* 1, 25–55.

Cady, S.L. and Farmer, J.D. (1996) Fossilization processes in silicious thermal springs: trends in preservation along the thermal gradient. In *Evolution of Hydrothermal Ecosystems on Earth (and Mars?): Ciba Foundation Symposium 202*, edited by G.R. Bock and J.A. Goode, John Wiley and Sons, Inc., Chichester, UK, pp. 150–173.

Cady, S.L., Farmer, J.D., Grotzinger, J.P., Schopf, J.W., and Steele, A. (2003) Morphological biosignatures and the search for life on Mars. *Astrobiology* 3, 351–368.

Clark, B.C., Morris, R.V., McLennan, S.M., Gellert, R., Jolliff, B., Knoll, A.H., Squyres, S.W., Lowenstein, T.K., Ming, D.W., Tosca, N.J., Yen, A., Christensen, P.R., Gorevan, S., Brückner, J., Calvin, W., Dreibus, G., Farrand, W., Klingelhöfer, G., Wänke, H., Zipfel, J., Bell, J.F., III, Grotzinger, J., McSween, H.Y., and Rieder, R. (2005) Chemistry and mineralogy of outcrops at Meridiani Planum. *Earth Planet. Sci. Lett.* 240, 73–94.

Cockell, C.S. and Lee, P. (2002) The biology of impact craters—a review. *Biol. Rev.* 77, 279–310.

Cockell, C.S., Lee, P., Osinski, G., Horneck, G., and Broady, P. (2002) Impact-induced microbial endolithic habitats. *Meteorit. Planet. Sci.* 37, 1287–1298.

Des Marais, D.J., Clark, B.C., Crumpler, L.S., Farmer, J.D., Grotzinger, J.P., Haskin, L.A., Knoll, A.H., Landis, G.A., Moersch, J., Schröder, C., Wdowiak, T., Yen, A.S., Squyres, S.W., and the Athena Science Team (2005) Astrobiology and the basaltic plains in Gusev Crater [abstract 2353]. In *36th Lunar and Planetary Science Conference Abstracts*, Lunar and Planetary Institute, Houston, available on CD-ROM.

Edwards, H.G.M, Russell, M.C., and Wynn-Williams, D.D. (1997) Fourier transform Raman spectroscopic and scanning electron microscopic study of cryptoendolithic lichens from Antarctica. *Journal of Raman Spectroscopy* 30, 685–690.

Edwards, H.G.M., Wynn-Williams, D.D., and Jorge Villar, S.E. (2004) Biological modification of haematite in Antarctic cryptoendolithic communities. *Journal of Raman Spectroscopy* 35, 470–474.

Edwards, H.G.M., Jorge Villar, S.E., Parnell, J., Cockell, C.S., and Lee, P. (2005a) Raman spectroscopic studies of cyanobacterial gypsum halotrophs and their relevance for sulphate deposits on Mars. *Analyst* 130, 917–923.

Edwards, H.G.M., Moody, C.D., Jorge Villar, S.E., and Wynn-Williams, D.D. (2005b) Raman spectroscopic detection of key biomarkers of cyanobacteria and lichen symbiosis in extreme Antarctic habitats: evaluation for Mars Lander missions. *Icarus* 174, 560–571.

Edwards, H.G.M., Jorge Villar, S.E., Pullan, D., Hargreaves, M.D., Hofmann, B.A., Westall, F. (2007) Morphological biosignatures from relict fossilised sedimentary geological specimens: a Raman spectroscopic study. *Journal of Raman Spectroscopy* 38, 1352–1361.

Ellery, A. and Wynn-Williams, D.D. (2003) Why Raman spectroscopy on Mars? A case for the right tool for the right job. *Astrobiology* 3, 565–579.

Erokhina, L.G., Shatilovich, A.V., Kaminskaya, O.P., and Gilichinskii, D.A. (2002) The absorption and fluorescence spectra of the cyanobacterial phycobionts of cryptoendolithic lichens in the high-polar regions of Antarctica. *Microbiology* 71, 601–607.

Fouke, B.W., Farmer, J.D., Des Marais, D.J., Pratt, L., Sturchio, N.L., Burns, P.C., and Discipulo, M.K. (2000) Depositional facies and aqueous-solid geochemistry of travertine-depositing hot springs (Angel Terrace, Mammoth Hot Springs, Yellowstone National Park, U.S.A.). *J. Sediment. Res. A Sediment Petrol. Process.* 70, 565–585.

Friedmann, E.I. (1982) Endolithic microorganisms in the Antarctic cold desert. *Science* 215, 1045–1053.

Friedmann, E.I., Hua, M.S., and Ocampo-Friedmann, R. (1988) Cryptoendolithic lichen and cyanobacterial communities of the Ross Desert, Antarctica. *Polarforschung* 58, 251–259.

Gilmore, M.S., Castano, R., Mann, T., Anderson, R.C., Mjolsness, E.D., Manduchi, R. and Saunders, R.S. (2000) Strategies for autonomous rovers at Mars. *J. Geophys. Res.* 105, 29223–29237.

Glazner, A.F. (1988) Stratigraphy, structure and potassic alteration of Miocene volcanic rocks in the Sleeping Beauty area, central Mojave Desert, California. *Geol. Soc. Am. Bull.* 100, 424–435.

Golombek, M.P. (1997) The Mars Pathfinder Mission. *J. Geophys. Res.* 102, 3953–3965.

Gorevan, S., Myrick, T., Batting, C., Mukherjee, S., Bartlett, P., and Wilson, J. (2003a) Strategies for future Mars exploration: an infrastructure for the near and long-term future exploration of the subsurface of Mars [abstract 3196]. In *6th International Conference on Mars (2003)*, Lunar and Planetary Institute, Houston.

Gorevan, S., Myrick, T., Davis, K., Chau, J.J., Bartlett, P., Mukherjee, S., Anderson, R., Squyres, S.W., Arvidson, R.E., Madsen, M.B., Bertelsen, P., Goetz, W., Binau, C.S., and Richter, L. (2003b) Rock Abrasion Tool: Mars Exploration Rover mission. *J. Geophys. Res.* 108, 8068.

Grieve, R.A.F. (1988) The Haughton impact structure: summary and synthesis of the results of the HISS project. *Meteoritics* 23, 249–254.

Griffiths, A.D., Coates, A.J., Josset, J.-L., Paar, G., Hofmann, B., Pullan, D., Rueffer, P., Sims, M.R., and

Pillinger, C.T. (2005) The Beagle 2 stereo camera system. *Planet. Space Sci.* 53, 1466–1482.

Grotzinger, J.P. and Knoll, A.H. (1999) Precambrian stromatolites: evolutionary milestones or environmental dipsticks? *Annu. Rev. Earth Planet. Sci.* 27, 313–358.

Grotzinger, J.P. and Rothman, D.H. (1996) An abiotic model for stromatolite morphogenesis. *Nature* 383, 423–425.

Hamilton, V.E. (2006) Spectral evidence for silica in Eos Chasma, Mars [abstract P22A-07]. In *American Geophysical Union, Fall Meeting 2006*, American Geophysical Union, Washington, DC.

Henry, D.J. (1957) *California Gem Trails*, Baldwin Park, California.

Hofmann, B.A. and Farmer, J.D. (2000) Filamentous fabrics in low-temperature mineral assemblages: are they fossil biomarkers? Implications for the search for a subsurface fossil record on the early Earth and Mars. *Planet. Space Sci.* 48, 1077–1086.

Hofmann, H.J., Grey, K., Hickman, A.H., and Thorpe, R.I. (1999) Origin of 3.45 Ga coniform stromatolites in Warrawoona Group, Western Australia. *Geol. Soc. Am. Bull.* 111, 1256–1262.

Hofmann, B.A., Josset, M., and Josset, J.-L. (2002) Imaging of Mars analogue materials using the Beagle 2 camera system. In *Proceedings of the Second European Workshop on Exo/Astrobiology, Graz, Austria, 2002*, ESA SP-518, European Space Agency, Paris, pp. 387–390.

Israel, E.J., Arvidson, R.E., Wang, A., Pasteris, J.D., and Joliff, B.L. (1997) Laser Raman spectroscopy of varnished basalt and implications for *in situ* measurements of martian rocks. *J. Geophys. Res.* 102, 28705–28716.

Jorge Villar, S.E., Edwards, H.G.M., Wynn-Williams, D.D., and Worland, M.R. (2003) FT-Raman spectroscopic analysis of an Antarctic endolith. *Int. J. Astrobiology* 1, 349–355.

Klingelhöfer, G., Morris, R.V., Bernhardt, B., Rodionov, D., de Souza, P.A., Jr., Squyres, S.W., Foh, J., Kankeleit, E., Bonnes, U., Gellert, R., Schröder, C., Linkin, S., Evlanov, E., Zubkov, B., and Prilutski, O. (2003) Athena MIMOS II Mössbauer spectrometer investigation. *J. Geophys. Res.* 108, 8097.

Klingelhöfer, G., Morris, R.V., Bernhardt, B., Schröder, C., Rodionov, D., de Souza, P.A., Jr., Yen, A., Gellert, R., Evlanov, E., Zubkov, B., Foh, J., Bonnes, U., Kankeleit, E., Gütlich, P., Ming, D.W., Renz, F., Wdowiak, T., Squyres, S.W., and Arvidson, R.E. (2004) Jarosite and hematite at Meridiani Planum from Opportunity's Mössbauer Spectrometer. *Science* 306, 1740–1745.

Knoll, A.H., Carr, M., Clark, B., Des Marais, D.J., Farmer, J.D., Fischer, W.W., Grotzinger, J.P., McLennan, S.M., Malin, M., Schröder, C., Squyres, S.W., Tosca, N.J., and Wdowiak, T. (2005) An astrobiological perspective on Meridiani Planum. *Earth Planet. Sci. Lett.* 240, 179–189.

Knudsen, J.M. (1989) Mössbauer Spectroscopy of ^{57}Fe and the evolution of the Solar System. *Hyperfine Interact.* 47, 3–31.

Knudsen, J.M., Mørup, S., and Galazkha-Friedman, J. (1990) Mössbauer spectroscopy and the iron on Mars. *Hyperfine Interact.* 57, 2231–2236.

Knudsen, J.M., Madsen, M.B., Olsen, M., Vistisen, L., Koch, C.B., Mørup, S., Kankeleit, E., Klingelhöfer, G., Evlanov, E.N., Khromov, V.N., Mukhin, L.M., Prilutski, O.F., Zubkov, B., Smirnov, G.V., and Juchniewicz, J. (1992) Mössbauer spectroscopy on the surface of Mars. Why? *Hyperfine Interact.* 68, 83–94.

Krumbein, W.E. (1983) Stromatolites—the challenge of a term in space and time. *Precambrian Res.* 20, 493–531.

Lowe, D.R. (1980) Stromatolites 3,400-Myr old from the Archaean of Western Australia. *Nature* 284, 441–443.

Lowe, D.R. (1994) Abiological origin of described stromatolites older than 3.2 Ga. *Geology* 22, 287–390.

Lowe, D.R. and Braunstein, D. (2003) Microstructure of high-temperature (>73°C) siliceous sinter deposited around hot springs and geysers, Yellowstone National Park: the role of biological and abiological processes in sedimentation. *Can. J. Earth Sci.* 40, 1611–1642.

Melchiorre, E.B. and Williams, P.A. (2001) Stable isotopic characterization of the thermal profile and subsurface biological activity during oxidation of the Great Australia Deposit, Cloncurry, Queensland, Australia. *Econ. Geol.* 96, 1685–1693.

Morris, R.V., Klingelhöfer, G., Bernhardt, B., Schröder, C., Rodionov, D., de Souza, P.A., Jr., Yen, A., Gellert, R., Evlanov, E., Foh, J., Kankeleit, E., Gütlich, P., Ming, D.W., Renz, F., Wdowiak, T., Squyres, S.W., and Arvidson, R.E. (2004) Mineralogy at Gusev Crater from the Mössbauer Spectrometer on the Spirit Rover. *Science* 305, 833–836.

Morris, R.V., Klingelhöfer, G., Schröder, C., Rodionov, D.S., Yen, A., Ming, D.W., de Souza, P.A., Jr., Fleischer, I., Wdowiak, T., Gellert, R., Bernhadrt, B., Evlanov, E.N., Zubkov, B., Foh, J., Bonnes, U., Kankeleit, E., Gütlich, P., Renz, F., Squyres, S.W., and Arvidson, R.E. (2006) Mössbauer mineralogy of rock, soil, and dust at Gusev crater, Mars: Spirit's journey through weakly altered basalt on the plains and pervasively altered basalt in the Columbia Hills. *J. Geophys. Res.* 111, E02S13, doi:10.1029/2005JE002584.

Osinski, G.R. and Spray, J.G. (2003) Evidence for the shock melting of sulfates from the Haughton impact crater, Artic Canada. *Earth Planet. Sci. Lett.* 215, 357–370.

Pache, M., Reitner, J., and Arp, G. (2001) Geochemical evidence for the formation of a large Miocene "Travertine" mound at a sublacustrine spring in a soda lake (Wallerstein Castle Rock, Nordlinger Ries, Germany). *Facies* 45, 211–230.

Parnell, J., Lee, P., Cockell, C.S., and Osinski, G.R. (2004) Microbial colonization in impact-generated hydrothermal sulphate deposits, Haughton impact structure, and implications for sulphates on Mars. *Int. J. Astrobiology* 3, 265–271.

Pohl, J., Stöffler, D., Gall, H., and Ernstson, K. (1977) The Ries Impact Crater. In *Impact and Explosion Cratering*, edited by D.J. Roddy, R.O. Pepin, and R.B. Merrill, Pergamon Press, New York, pp. 343–404.

Pohl, J., Eckstaller, A., and Robertson, P.B. (1988) Gravity and magnetic investigations in the Haughton impact structure, Devon Island, Canada. *Meteoritics* 23, 235–238.

Poulet, F., Bibring, J.-P., Mustard, J.F., Gendrin, A., Mangold, N., Langevin, Y., Ardvison, R.E., Gondet, B., and Gomez, C. (2005) Phyllosilicates on Mars and implications for early martian climate. *Nature* 438, 623–627.

Pullan, D., Sims, M.R., Wright, I.P., Pillinger, C.T. and Trautner, R. (2003) Beagle 2: the exobiological lander of Mars Express. In *Mars Express: The Scientific Payload*, ESA SP-1240, edited by A. Wilson, European Space Agency, Paris.

Ramsey, M.H., Potts, P.J., Webb, P.C., Watkins, P., Watson, J.S., and Coles, B.J. (1995) An objective assessment of analytical method precision: comparison of ICP-AES and XRF for the analysis of silicate rocks. *Chem. Geol.* 124, 1–19.

Richter, L., Coste, P., Gromov, V.V., Kochan, H., Nadalini, R., Ng, T.C., Pinna, S., Richter, H.-E., and Yung, K.L. (2002) Development and testing of subsurface sampling devices for the Beagle 2 lander. *Planet. Space Sci.* 50, 903–913.

Rieder, R., Economou, T., Wänke, H., Turkevich, A., Crisp, J., Brückner, J., Dreibus, G., and McSween, H.Y., Jr. (1997) The chemical composition of martian soil and rocks returned by the mobile alpha proton X-ray spectrometer: preliminary results from the X-ray mode. *Science* 278, 1771–1774.

Rothschild, L.J. and Mancinelli, R.L. (2001) Life in extreme environments. *Nature* 409, 1092–1101.

Ruiz, J.M.G, Carnerup, A., Christy, A.G., Welham, N.J., and Hyde, S.T. (2002) Morphology: an ambiguous indicator of biogenicity. *Astrobiology* 2, 335–351.

Sangameshwar, S.R. and Barnes, H.L. (1983) Supergene processes in zinc-lead-silver sulphide ores in carbonates. *Econ. Geol.* 78, 1379–1397.

Schenker, P.S., Huntsberger, T.L., Pirjanian, P., Baumgartner, E.T., and Tunstel, E. (2003) Planetary developments supporting Mars exploration, sample return and future human-robotic colonization. *Auton. Robots* 14, 103–126.

Schröder, C., Klingelhöfer, G., and Tremel, W. (2004) Weathering of Fe-bearing minerals under Martian conditions, investigated by Mössbauer spectroscopy. *Planet. Space Sci.* 52, 997–1010.

Schröder, C., Klingelhöfer, G., Bailey, B., and Staudigel, H. (2005) Mössbauer spectroscopy as a tool in astrobiology. *Hyperfine Interact.* 166, 567–571.

Scott, D. and Hajnal, Z. (1988) Seismic signature of the Haughton structure. *Meteoritics* 23, 239–247.

Sharma, S.K., Lucey, P.G., Ghosh, M., Hubble, H.W., and Horton, K.A. (2003) Stand-off Raman spectroscopic detection of minerals on planetary surfaces. *Spectrochim. Acta A Mol. Biomol. Spectrosc.* 59, 2391–2407.

Sherlock, S.C., Kelley, S.P., Parnell, J., Green, P., Lee, P., Osinski, G.R., and Cockell, C.S. (2005) Re-evaluating the age of the Haughton impact crater. *Meteorit. Planet. Sci.* 40, 1777–1787.

Siebert, J., Hirsch, P., Hoffmann, B., Gliesche, C.G., Peissl, K., and Jendrach, M. (1996) Cryptoendolithic microorganisms from Antarctic sandstone of Linnaeus Terrace (Asgard Range): diversity, properties and interactions. *Biodivers. Conserv.* 5, 1337–1363.

Sims, M.R., Cullen, D.C., Bannister, N.P., Grant, W.D., Henry, O., Jones, R., McKnight, D., Thompson, D.P., and Wilson, P.K. (2005) The specific molecular identification of life experiment (SMILE). *Planet. Space Sci.* 53, 781–791.

Squyres, S.W. and Knoll, A.H. (2005) Sedimentary rocks at Meridiani Planum: origin, diagenesis, and implications for life on Mars. *Earth Planet. Sci. Lett.* 240, 1–10.

Squyres, S.W., Arvidson, R.E., Baumgartner, E.T., Bell, J.F., III, Christensen, P.R., Gorevan, S., Herkenhoff, K.E., Klingelhöfer, G., Madsen, M.B., Morris, R.V., Rieder, R., and Romero, R.A. (2003) Athena Mars rover science investigation. *J. Geophys. Res.* 108, 8062.

Sumner, D.Y. (2004) Poor preservation potential of organics in Meridiani Planum Unit P2 sedimentary rocks. In *Mars Astrobiology Science and Technology Workshop*, Washington, DC.

Sun, H.J. and Friedmann, E.I. (1999) Growth on geological time scales in the Antarctic cryptoendolithic microbial community. *Geomicrobiol. J.* 16, 193–202.

Talboys, D.L. (2006) The Beagle 2 X-ray spectrometer for Mars. PhD thesis, University of Leicester, UK.

Tarcea, N., Popp, J., Schmitt, M., Kiefer, W., Hochleitner, R., Simon, G., Hilchenbach, M., Hofer, S., and Stuffler, T. (2002) Raman spectroscopy as a suitable tool for biological and mineralogical *in situ* planetary studies. In *Proceedings of the Second European Workshop on Exo/Astrobiology, Graz, Austria, 2002*, ESA SP-518, European Space Agency, Paris, pp. 399–402.

Thomas, N., Lüthi, B.S., Hviid, S.F., Keller, H.U., Markiewicz, W.J., Blümchen, T., Basilevsky, A.T., Smith, P.H., Tanner, R., Oquest, C., Reynolds, R., Josset, J.-L., Beauvivre, S., Hofmann, B., Rüffer, P., and Pillinger, C.T. (2004) The microscope for Beagle 2. *Planet. Space Sci.* 52, 853–866.

Vago, J.L., Gardini, B., and Kminek, G. (2003) ESA's new mission to search for signs of life on Mars: ExoMars and its Pasteur scientific payload. EGS-AGU-EUG joint assembly, Nice, France, 6–11 April 2003, European Geophysical Society, *Geophysical Research Abstracts* 5, 02504.

Walker, J.J., Spear, J.R., and Pace, N.R. (2005) Geobiology of a microbial endolithic community in the Yellowstone geothermal environment. *Nature* 434, 1011–1014.

Walter, M.R. (1978) Recognition and significance of Archaean stromatolites. In *Archaean Cherty Metasediments: Their Sedimentology, Micropalaeontology, Biogeochemistry, and Significance to Mineralization*, edited by J.E. Glover and D.I. Groves, University of Western Australia, Perth, WA, pp. 1–10.

Walter, M.R., Buick, R., and Dunlop, J.S.R. (1980) Stromatolites 3400–3500 Myr old from the North Pole area, Western Australia. *Nature* 284, 443–445.

Wang, A., Haskin, L.A., Lane, A.L., Wdowiak, T.J., Squyres, S.W., Wilson, R.J., Hovland, L.E., Manatt, K.S., Raouf, N., and Smith, C.D. (2003) Development of the Mars microbeam Raman spectrometer (MMRS). *J. Geophys. Res.* 108, 5005.

Westall, F. (2005a) Life on the early Earth: a sedimentary view. *Science* 308, 366–367.

Westall, F. (2005b) Early life on Earth and analogies to Mars. In *Water on Mars and Life*, edited by T. Tokano, Adv. Astrobiol. Biogeophys., Springer, Berlin Heidelberg, pp. 45–64.

Wierzchos, J., Ascaso, C., Sancho, L.G., and Green, A. (2003) Iron-rich diagenetic minerals are biomarkers of microbial activity in Antarctic rocks. *Geomicrobiol. J.* 20, 15–24.

Wilson, A., editor. (1999) *Exobiology in the Solar System and the Search for Life on Mars*, *European Space Agency, SP-1231*, ESA Publications Division, ESTEC, Noordwijk, The Netherlands.

Wynn-Williams, D.D. and Edwards, H.G.M. (2000) Proximal analysis of regolith habitats and protective biomolecules *in situ* by laser Raman spectroscopy: overview of terrestrial Antarctic habitats and Mars analogs. *Icarus* 144, 486–503.

Address reprint requests to:
Derek Pullan
Space Research Centre
Department of Physics and Astronomy
University of Leicester
University Road
Leicester LE1 7RH, UK

E-mail: dpu@star.le.ac.uk